

POLITECNICO DI TORINO

DIPARTIMENTO DI INGEGNERIA MECCANICA E
AREOSPAZIALE (DIMEAS)



SPAULDINGTM
REHABILITATION HOSPITAL



HARVARD
MEDICAL SCHOOL

Master's Degree Thesis in Biomedical Engineering

Using Deep Learning-Based Pose Estimation Algorithms for Markerless Gait Analysis in Rehabilitation Medicine

Supervisors

Prof. Danilo DEMARCHI

Prof. Paolo BONATO

Candidate

Rosita RABBITO

Torino, March 2021

Abstract

Walking is one of the most natural human activities and certainly the most impactful on one's quality of life. However, the human ability to walk can be compromised by neurological, orthopedic, or traumatological factors. When the gait is impaired by one or multiple of these factors, a key objective of modern rehabilitation interventions is to help people with gait impairments to regain or improve their ability to walk, minimizing the negative impact on their quality of life at both a social and personal level.

Nowadays, gait analysis laboratories use multiple technologies to evaluate and improve the individual's gait patterns. Among the various tools available for gait analysis, Motion Capture systems based on cameras and infrared-reflective markers positioned on the individual are used as gold standard, due to their high accuracy. However, these systems have the disadvantage of being cumbersome, costly, complex, and not time-efficient.

The proposed study aims at using a new motion detection approach that relies on deep learning-based algorithms with the long-term goal of providing a simple, cost and time-effective alternative to motion analysis systems currently used in rehabilitation medicine.

In this study, five healthy subjects without any motor disabilities were recruited and asked to walk on a treadmill at different speeds to collect video data. The collection of this data has made it possible to carry out the biomechanical analysis of movement and the estimation of biomechanical parameters of clinical interest both using the gold standard gait analysis system and using the modern system based on machine learning. All this made it possible to compare the gait parameters extracted through the two tracking motion systems, OpenPose, and Vicon.

The objective of the thesis is the comparison of these two motion tracking tools with particular focus on the joint angles of the lower limbs, specifically the angles of the hip, knee, and ankle, on the position of the centers of joint rotation and on the fundamental kinematic parameters of the gait cycle. We quantify the error in terms of the shape of the trajectories of the body joints, their displacement, and the shape and magnitude of the angles.

To cope with the purpose of this work, there are preliminary stages of processing the data extracted from the two systems. A simplified biomechanical model was developed to allow the calculation of the angles characterizing the lower limb through the data extracted from the OpenPose system.

The obtained results show a high correlation between the hip and knee angles extracted with the two systems with a Root Mean Square Error (RMSE) below 5 degrees and a Mean Absolute Error (MAE) below 4 degrees. The comparison between the ankle angles obtained by the two systems show an RMSE below 8.5 degrees, an MAE below 6.5 degrees, and a correlation index greater than 0.5 for all the subjects analyzed. The cause for the major error

obtained in the ankle angle is due to an inaccurate estimate of the foot key-points during the subject's walking by the OpenPose pose estimation tool.

In conclusion, it can be said that the OpenPose system has great potential for its application in rehabilitation medicine. However, further investigation and improvements are needed to make it more robust and to allow its use even with people who have motor disabilities.

Acknowledgement

I am very keen to thank my supervisor, Professor Danilo Demarchi, who believed in me and in my abilities and who allowed me to have the opportunity to meet and work with the staff of Motion Analysis Lab of Spaulding Hospital and Harvard Medical School in Boston. I am also very grateful to Professor Paolo Bonato who chose and guided me for all twelve months of work, his role as mentor was fundamental for the success of this project and for my professional growth, and I also thank him because despite the situation world emergency has allowed me to work with him and his staff. In this regard, I would like to thank all the staff, but in particular, Federico Parisi who followed me in all my choices and always supported, encouraged, and advised me in the best way with exceptional passion and dedication.

The most special thanks go to my family, my mother, my father, and my brother, because thanks to them, their support, their lessons, and criticisms but above all their unconditional love they have always encouraged me to express myself better and to achieve all my goals. I thank them infinitely for all they have done and do every day for me.

I thank my dearest uncles, Mariella and Corrado, my little cousins, and all my grandparents for the love, support, and life teachings but above all the happiness they have always expressed for every little step I take.

Finally, I thank the closest friends, of a lifetime or known along my course of study, those who have always rejoiced and celebrated with me and for me.

To my guardian angel,

To my family,

To my future.

Contents

List of Table	IX
List of Figures	X
Acronyms	XIII
1 Introduction	1
1.1 Clinical Relevance.....	1
1.2 Aim of the thesis	2
2 Introduction to Gait Analysis	3
2.1 Gait Cycle.....	3
2.2 Joints of lower limb.....	5
2.3 Parameters	7
2.3.1 Spatio-temporal Parameters	7
2.3.2 Kinematics Parameters	8
2.3.3 Kinetics Parameters.....	9
3 Technologies and Systems for Gait Analysis.....	10
3.1 State of the art	10
3.2 VICON	12
3.2.1 Hardware components.....	13
3.2.2 Software and processing steps.....	15
3.3 OPENPOSE.....	17
3.3.1 The overall pipeline of OpenPose	18
3.3.2 Use of OpenPose	20
4 Materials and Methods	22
4.1 Protocol	22
4.1.1 Data collection procedure.....	23
4.1.2 Extracted information.....	24

4.2	Rectification of the video	25
4.3	Data Analysis	28
4.3.1	New Reference System	29
4.3.2	Conversion from Meter to Pixel.....	30
4.3.3	Biomechanical models for computing the angles	31
4.3.3.1	Angles definition using the original biomechanical model	31
4.3.3.2	Angles definition using the simplified biomechanical model.....	32
4.3.4	Processing OpenPose Data.....	35
5	Results and Discussion.....	38
5.1	Validation of the simplified biomechanical model	38
5.2	Joint center position	45
5.3	Angles of the lower limb	50
5.4	Kinematics Parameters	58
6	Conclusion and Future Goals	62
	Bibliography.....	65

List of Table

Table 4.1 - Subjects general information.	22
Table 4.2 - Selected speed for each session of walking trial on the treadmill.	23
Table 4.3 - Lens Parameters obtained with the camera calibration Matlab tool.....	27
Table 4.4 - Treadmill length in meters and pixels and conversion factor from meters to pixels for all five subjects.	30
Table 4.5 - Shows the values of the window length used for the median filter and the cut-off frequencies chosen, for each subject.	35
Table 5.1 - The average distance for hip angle and ankle angle for all the five subjects.....	42
Table 5.2 - Average RMSE values of the angles of the lower limb for each subject.	44
Table 5.3 - Mean value, standard deviation, maximum and minimum values of the mean absolute error between the Vicon angles and the angles calculated with the created biomechanical model using the coordinates of the joints extracted with the Vicon system. ...	44
Table 5.4 - Distance, in centimeters, between the OpenPose landmarks and the Vicon joints.	46
Table 5.5 -Euclidean distance, in centimeters, of the OpenPose landmarks and the Vicon joints.	47
Table 5.6 - Euclidean distance after the error compensation.	48
Table 5.7 - Pearson correlation index between the trajectories of the landmarks, both along the x and y-axis, of the two motion tracking tools.	49
Table 5.8 – Average values of MAE between Vicon and OpenPose angles.	55
Table 5.9 – Average RMSE values obtained from Vicon and OpenPose angles.....	55
Table 5.10 - Average Pearson Coefficient values obtained from Vicon and OpenPose angles.	56
Table 5.11 - MAE of the values of the kinematic parameters obtained from the corners of the lower limb extracted with the two systems of motion tracking.	60
Table 5.12 - MAE of the position in the GC of the kinematic parameters of the angles of the two system.....	60

List of Figures

Figure 2.1 - Phases division of Gait Cycle [25].	4
Figure 2.2 - The human body in standard position and anatomical plane: a) Frontal plane, b) Sagittal plane, c) Transverse plane.	5
Figure 2.3 - Example of the possible movements of the joints.	7
Figure 2.4 - Kinematic curves of the hip, knee, and ankle joint in the sagittal plane and for each of them the main parameters are indicated.	9
Figure 3.1 - Active Vicon Wand [16].	13
Figure 3.2 - Example of passive markers	14
Figure 3.3 - Location of Vicon cameras used in the laboratory and volume of motion they consider.	15
Figure 3.4 - Marker structure and labels on Vicon Nexus.	16
Figure 3.5 - Visual3D picture.	17
Figure 3.6 - Overall pipeline of OpenPose method [13].	18
Figure 3.7 - Multi-stage Convolutional Neural Network architecture [13].	18
Figure 3.8 - OpenPose Body Model: a) BODY-25, b) COCO [13].	20
Figure 3.9 - Example of a frame from the static test video taken on one of the subjects examined with the skeleton extracted using OpenPose estimation tool.	21
Figure 4.1 - Explanation of the role of intrinsic and extrinsic parameters.	25
Figure 4.2 - Example of used input-image with the chessboard.	26
Figure 4.3 - Workflow for video rectification.	26
Figure 4.4 - The frame of a video of the walking-trial at Slow speed for Subject 2. In a) the original frame, in b) the rectified frame.	27
Figure 4.5 - Pipeline of processing data.	28
Figure 4.6 - Shows in red the new system of reference that has origin in marker in the front part of the treadmill (A2), in black the VICON system, in blu the OPENPOSE system in the lateral view and in green the position of the marker in the back part of the treadmill (A1).	29
Figure 4.7 - Depiction of the biomechanical definition of the angles of the hip, knee and ankle in the lateral view [18].	32
Figure 4.8 - The proposed simplified biomechanical model.	34

Figure 4.9 - Example of an outlier that persists after using the median filter and how the signal is reconstructed with the method explained. The steps are: a) identification of outliers, b) elimination, c) signal reconstruction. A portion of the X-coordinate signal of subject 4's knee is shown during the first slow speed walking session.....	36
Figure 4.10 - Example of result obtained on signals after filtering them with the median and low pass filter and after applying the outliers removal method. The figure shows the data of the subject 2 in the first Fast speed session.....	37
Figure 5.1 - Angles of hip, knee and ankle provided by Vicon system of Subject 1	39
Figure 5.2 - Hip, Knee and Ankle angles extracted with the Proposed Method starting from the position of the joints by Vicon of Subject 1.....	39
Figure 5.3 - Angles of hip, knee and ankle provided by Vicon system of Subject 5.....	40
Figure 5.4 - Hip, Knee and Ankle angles extracted with the Proposed Method starting from the position of the joints by Vicon of Subject 5.....	40
Figure 5.5 - Angles of the Lower Right Limb provided by Vicon, in blue, and angles provided by the Biomechanical model created in this thesis, in magenta (Subject 1).....	41
Figure 5.6 - Angles of the Lower Right Limb provided by Vicon, in blue, and angles provided by the Biomechanical model created in this thesis, in magenta (Subject 5).....	41
Figure 5.7 - Hip, Knee, and Ankle angles of the Vicon system, in blue, and corrected angles, with the adjusted offset, obtained with the method used in this thesis, in magenta (Subject 1).	42
Figure 5.8 - Hip, Knee, and Ankle angles of the Vicon system, in blue, and corrected angles, with the adjusted offset, obtained with the method used in this thesis, in magenta (Subject 5)	43
Figure 5.9 - RMSE calculated for each step (Subject 1).....	43
Figure 5.10 - RMSE calculated for each step (Subject 5).....	43
Figure 5.11 - Comparison between Vicon, in blue, and OpenPose, in red, Neck coordinates along x and y axis (Subject 1).....	47
Figure 5.12 - Comparison between the coordinates, along the y-axis of Ankle, Heel, Median Toe and Lateral Toe, Vicon, in blue, and OpenPose, in red. (Subject 1).....	48
Figure 5.13 - Vicon angles of the lower limb (Subject 2).....	51
Figure 5.14 - OpenPose angles of the lower limb (Subject 2).....	51
Figure 5.15 - Vicon angles of the lower limb (Subject 3).....	51
Figure 5.16 - OpenPose angles of the lower limb (Subject 3).....	52
Figure 5.17 - Hip, Knee and Ankle angles obtained by Vicon system, in blue, and OpenPose angles, in red (Subject 2).....	52
Figure 5.18 - Median distance, in black, and standard deviation, in grey, between the angles provided by the two systems (Subject 2).....	53

Figure 5.19 – Lower limb angles obtained by Vicon system, in blue, and OpenPose angles, in red (Subject 3).	53
Figure 5.20 - Median distance, in black, and standard deviation, in grey, between the angles provided by the two systems (Subject 3).	53
Figure 5.21 – MAE of the Hip angles of all subject in the different speed level of walking trial.	54
Figure 5.22 – MAE of the Knee angles of all subject in the different speed level of walking trial.	54
Figure 5.23 - MAE of the Ankle angles of all subject in the different speed level of walking trial.	55
Figure 5.24 - Fit curves and goodness-of fit info for the angles of hip, knee, and ankle of the two systems for subject 1.	56
Figure 5.25 - Comparison of the Kinematic Parameters for the subject 3. In blue the curves of the angles extracted with the Vicon system and in dark blue dots the parameters are highlighted, in light blue the curves and parameters obtained with the data extracted from the OpenPose system.	59
Figure 5.26 - MAE values obtained by comparing the extracted parameters values for the angles of the two systems for the subject 3.	60

Acronyms

GA	Gait Analysis
GC	Gait Cycle
2D	Two dimensions
3D	Three dimensions
IC	Initial Contact
LR	Loading Response
MST	Mid-Stance
TST	Terminal Stance
PSW	Pre-Swing
ISW	Initial Swing
MSW	Mid-Swing
TSW	Terminal Swing
LED	Light-emitting diode
EMG	Electromyography
DOF	Degrees of Freedom
IIR	Infinite Impulse Response
RHS	Right Heel Strike
RTO	Right Toe Off
RMSE	Root Mean Square Error
MAE	Mean Absolute Error

Chapter 1

1 Introduction

1.1 Clinical Relevance

The use of gait analysis (GA) is still of fundamental importance today in both clinical and research fields.

Walking is the most natural and common motor activity for the individual even if in reality it is a complex action that involves most of the joints in the body.

GA is defined as the process of analyzing the kinetic, kinematic, and spatial-temporal parameters of gait in people with both normative and impaired walking.

In fact, this type of analysis is used, on a clinical level, especially in the rehabilitation of patients who have been affected by neurological diseases such as polyneuropathies, cerebral stroke, Parkinson's disease, multiple sclerosis, etc., or from orthopedic diseases, as it provides the objective data to which experts refer to set up recovery strategies or gait prevention programs.

The major gait analysis laboratories use as gold standard systems based on cameras and infrared markers, positioned on the key anatomical sites of the lower limbs or of the entire body, which allow immediate processing of data concerning the pose and movement of the subject under examination using techniques based on biomechanical models. Although the accuracy of the data that is estimated by these systems is irrefutable, there are several disadvantages.

First, the cost of the system is high, and this limits its use and the feasibility of this analysis. The positioning of the markers is complex and time-consuming and must be done by specialized personnel, as the results strongly depend on it, but it is even more complicated in those patients who have physical disabilities. In addition, between the preparation of the subject and the obtaining of the results, a period of about two or more hours elapses.

Precisely for these negative aspects, today more than ever, new techniques for human pose estimation, mostly based on machine-learning algorithms have been developed and have attracted the attention of the scientific community. These systems could replace traditional gait analysis techniques in certain scenarios, precisely because in addition of being low-cost they are portable and not cumbersome but above all, they do not require the use of

markers to identify key-points in the human body , thus reducing the time required to perform the analysis.

1.2 Aim of the thesis

The idea for this work comes from the collaboration with the Motion Analysis Lab of Spaulding Hospital and Harvard Medical School in Boston.

The goal is to compare the accuracy of modern Motion Tracking systems based on Deep-Learning algorithms and traditional systems and investigate the performance discrepancy between the two, with the intent of assessing the suitability of this kind of markerless pose estimation systems for clinical gait analysis.

The novel system enables the identification of the human pose, or the joints of the human body, without using markers in videos or images and is often used in games or animations. Using video-cameras, the movement of interest can be recorded and then the 2D coordinates of the joints are extracted with the application of deep-learning algorithms.

Our aim is to extract through these new techniques the coordinates of the joints during walking and then calculate the kinematic parameters of interest, such as hip angle, knee angle and ankle angle, through biomechanical models. These kinematic data will be compared with the gait analysis parameters extracted using traditional systems.

In addition to the direct comparison between these two systems, we also aim at improving the accuracy of the markerless systems in order to understand the limits of this approach and evaluate its applicability in the clinic. In fact, the possibility of using such systems in gait analysis laboratories would bring many advantages, such as:

- a more efficient use of time when performing analyses on patients with motor disabilities, as the elimination of the marker placing procedure would speed-up the clinical routine,
- considerable cost reduction by laboratories because these systems are often open-source and can work with any type of RGB cameras.

In this work the Vicon system was used as the gold standard and the real-time pose estimation tool OpenPose as markerless pose estimation system.

The comparison between the marker-based motion acquisition system and the markerless posture estimation tool is based on:

- the biomechanical model used in terms of joint angles,
- position of the centers of joint of the lower limb,
- and define the error as a function of the gait: of the amplitude and magnitude of the angles and the position of the key-joints.

Chapter 2

2 Introduction to Gait Analysis

2.1 Gait Cycle

The walking of the human being is achieved through the movement of the pelvic limbs in an alternating and rhythmic way allowing the movement of the body and is divided into steps. Human locomotion is achieved through the activation of muscles, especially of the lower limbs, but also requires the functioning of the sensory information of the neuronal network to allow joint movement and control of muscle contraction despite being a spontaneous activity that requires little attention in everyday life.

The fundamental unit of walking is the step that uses the limbs alternately and cyclically during the walk to move the body but also to maintain, at the same time, the stability of the upright position.

During each step, one lower limb propagates forward while the other acts as a support and then reverse the roles. The gait cycle (GC) is defined as the period between the initial contact of the foot with the ground until the next contact of the same foot [1].

As shown in Figure 2.1, the GC is divided into two main phases:

- 1- The Stance Phase: begins with the initial contact of the foot on the ground and represents the period of adjacency on the ground where it supports all or part of the body weight. In a healthy adult, it accounts for approximately 62% of the entire walking cycle.
- 2- The Swing Phase: occupies the remaining percentage of the gait cycle (38%) and represents the period in which the foot is not resting on the ground but is in the air and the leg extends towards the next foot contact. It is therefore associated with the advancement of the limbs.

The two main phases are divided into eight sub-events [2] that are characterized by specific biomechanical functions and that allow the functional analysis of different events that occur in individual joints and consents the interpretation of possible abnormalities in the subject's walking.

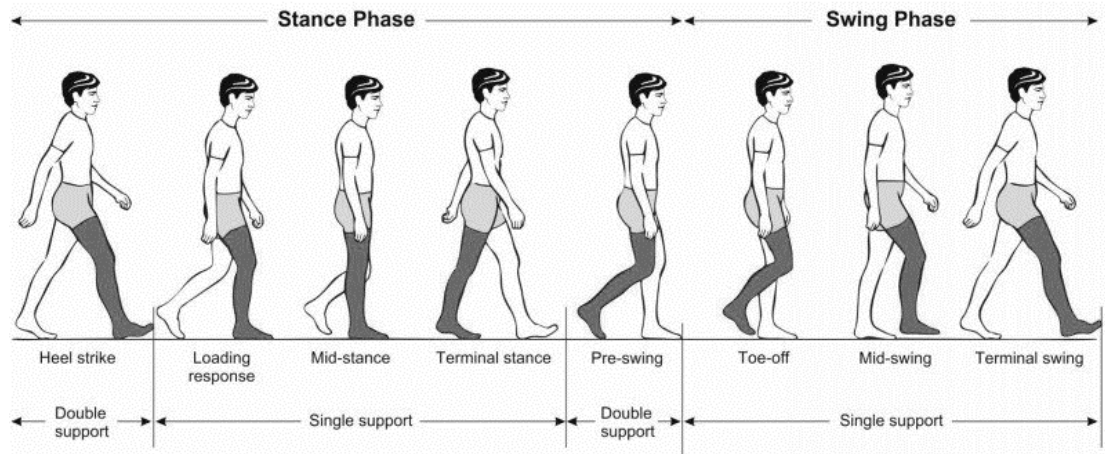


Figure 2.1 - Phases division of Gait Cycle [25].

The stance phase is divided into five sub-phases:

- Initial Contact (IC): it begins when the foot touches the ground, in healthy subjects, this occurs through the use of the heel (Heel Strike), and continues until the sole of the foot is completely in contact with the ground (Flat Foot). It represents the moment in which the center of mass is in its lowest position and at the joint level the knee is extended, the hip flexed, and the ankle dorsiflexed.
- Loading Response (LR): Start with the Flat Foot and continue until the opposite foot lifts. In this period, the knee flexion is due to the limb's cushioning response because the weight of the body is transferred to the forelimb. There is plantar flexion of the ankle and the hip is still flexed.
- IC and LR form the period defined as the weight acceptance which goes from the beginning up to 12% of the CG.
- Afterward begins the Single limb support period, where only one lower limb is responsible for body weight, which events are:
 - Mid-Stance (MST): where the swinging limb exceeds the supporting foot, the center of mass is at its highest point. Knee and hip begin to extend, and the ankle is dorsiflexed. This step ranges from 12% to 31% of the GC.
 - Terminal Stance (TST): it goes from 31% to 50% of the GC that is from the lifting of the heel until the contact of the opposite foot with the ground. The calf pushes inciting plantar flexion of the ankle, the knee extends again and then flexes slightly and the hip is more extended.
 - Pre-Swing (PSW): it is the final phase of the stance period, also known as the weight transfer phase, where the foot comes off the ground (Toe-Off) and comprises 50-62% of the GC. It involves greater knee flexion and planta-flexion of the ankle but also a loss of hip extension.

The swing phase consists of three sub-events:

- Initial Swing (ISW): it is a period of acceleration (62-75% GC) because the limb advances by lifting the foot through flexion of the hip and greater flexion of the knee. The ankle is slightly dorsiflexed.
- Mid-Swing (MSW): begins when the two limbs, swinging and supporting, are aligned and ends with the first one forward with respect to the second (75-87% GC). There is further flexion of the hip, the knee is extended, and the ankle continues to dorsiflex.
- Swing Terminal (TSW): it is the final phase of the swing but also of the deceleration and goes from 87% to the end of the overall cycle. The advancement of the limb is completed by flexing the knee and ends when the foot hits the ground and is in preparation for the subsequent support. The hip is flexed, and the ankle is dorsiflexed in a neutral position.

The PSW, ISW, MSW, and TSW events together form the limb advancement phase.

2.2 Joints of lower limb

In order to obtain an accurate movement analysis, it is important to describe the characteristics of the lower limbs in the three anatomical planes. The latter are described starting from the standard anatomical position of the human body defined as that position in which the subject is placed in an upright position with the head, palms and feet directed forward, with the arms held at the sides of the body, the heels together and the toes of the feet in contact as shown in Figure 2.2.

The sagittal plane is defined as the ideal plane that passes through the longitudinal axis of the body dividing it into two symmetrical parts right and left, the coronal plane is perpendicular to the previous plane, parallel to the forehead, and divides the body into the anterior and posterior parts. In conclusion, the transverse plane is parallel to the horizontal, perpendicular to the other two planes and divides the body into the upper and lower part.

In addition to the description of the body in the anatomical planes, it is of fundamental importance to describe the joints and segments of the lower limbs.

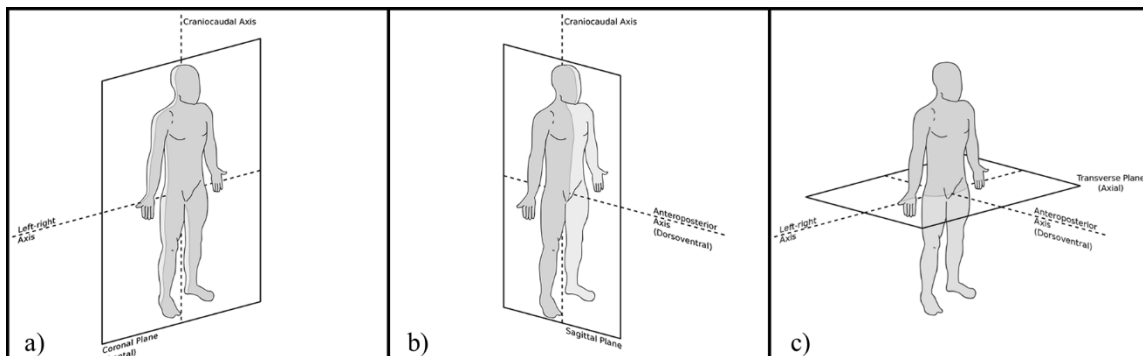


Figure 2.2 - The human body in standard position and anatomical plane: a) Frontal plane, b) Sagittal plane, c) Transverse plane.

The three segments are:

- the thigh is the proximal segment between the hip and knee joints,
- the shank is the intermediate segment between knee and ankle,
- the foot is the most distal segment of the limb and includes the joints between the 26 bones that make it up.

The joints are:

1- Hip Joint

The hip joint allows large movements as it can be assimilated to a spherical hinge with three degrees of freedom. It consists of the femoral head articulated in the acetabulum of the pelvis. To this joint it is allowed a greater flexion-extension movement in the sagittal plane (0-140 ° flexion and 0-15 ° extension) and reaches the maximum flexion in this plane during the swing phase, however, it reaches the maximum extension only when there is the foot detachment during the gait cycle [3].

On the frontal plane, abduction and adduction of approximately 0-25 ° and 0-30 °, respectively, are permitted [3]. In the oscillation phase, there is abduction and after reaching its maximum this is converted into adduction until the end of the support phase.

In the transverse plane, both internal and external rotation is permitted. The hip is almost always rotated internally during the entire stance phase and rotates externally at the end of this phase and then remains in this position for the entire second phase.

2- Knee Joint

This joint is composed of two joints, the tibiofemoral between the femur and tibia and the patellofemoral between the femur and patella. The first joint allows movement in all three planes, however, the one with the greatest value is in the sagittal plane which permits flexion-extension from 0 ° to 140 ° [4]. The movements in the transverse and frontal planes depend on the position that the joint has in the sagittal plane.

During walking, the knee has a flexion-extension range between about 0 ° and 70 °, there is an extension in the sagittal plane and maximum abduction in the frontal plane at the beginning of the stance phase and maximum flexion in the MSW phase [4]. External rotation in the transverse plane begins during knee extension in the stance phase and then reaches its maximum at the end of the swing phase. In correspondence with the flexion in the swing phase, there is an internal rotation in the transverse plane and adduction in the frontal plane.

3- Ankle Joint

The term ankle identifies the set of three joints: the tibiotarsal joint, the proximal tibiofibular joint, and the distal tibiofibular joint. The first is the junction point of the tibia, fibula, and talus and has only one degree of freedom allowing dorsal flexion (positive values) and plantar flexion (negative values) in the sagittal plane.

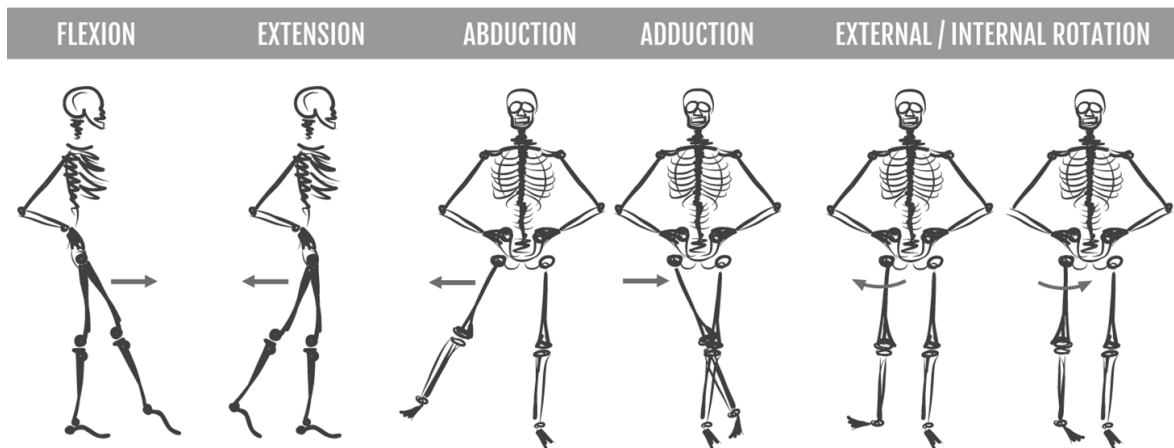


Figure 2.3 - Example of the possible movements of the joints.

2.3 Parameters

Using gait analysis, various kinetic, kinematic and spatio-temporal parameters can be extracted that are supportive to understand a patient's disabilities both at the neurological and orthopedic level. These objective data are incredibly valuable and widely used in many clinical applications, such as the definition of intervention strategies and post-operative treatment plans.

These are parameters that have great application in the clinical world as they are related to certain walking events.

2.3.1 Spatio-temporal Parameters

Cadence: number of steps taken in a given time (usually referred to the minute).

Step Length: longitudinal distance from the support of one foot to the support of the contralateral foot.

Step time: is the time taken for one step.

Stride Length: longitudinal distance from the support of one foot to the next ipsilateral support.

Stride time: it is the time spent for one stride.

Walking speed: is the distance traveled in a given time, the average one is basically the product between the cadence and the length of the stride.

Obviously, the speed depends on the length which in turn depends above all on the duration of the oscillation phase on each side [2].

Support time for single limb: is the time in which the foot touches the ground during the GC.

Support time of the double limb: is the elapsed time during which both feet are in support during the GC.

Stance-to-swing ratio: is the ratio between the two macro-phases of the gait cycle.

Obviously, they are informative parameters on the walking of the subject in question and very useful for evaluating treatments such as rehabilitation and diagnosis, however, taking into account only these spatio-temporal parameters does not allow to understand the cause or origin of the anomalies. Precisely for this reason, they must be accompanied by other evaluations.

2.3.2 Kinematics Parameters

Kinematic analysis studies the movement of bodies without considering the forces that these bodies exchange or the forces that cause such movements [5]. The parameters resulting from this type of analysis mainly measure the angles of the joints in the three anatomical planes.

Angles in the sagittal or frontal plane are usually more significant for gait analysis as they are easier to extract through observation-based techniques, in fact, the angles on the transverse plane can be confused with problems on the sagittal and/or coronal planes. Clearly, this does not happen when are used techniques based on infrared cameras and markers as they allow to have three-dimensional information.

Angular movements in the sagittal plane show: flexion-extension of the hip and knee and dorsiflexion or planta-flexion of the ankle.

On the frontal plane, there are abduction and adduction of the hip and knee.

On the transverse plane, there are the angular rotational movements of the joints of the lower limb.

The angular values at specific moments of the step cycle can be of fundamental importance because they add information on specific kinematic models related to neurological or orthopedic diseases [6]. Figure 2.4 shows an example of possible kinematics parameters of the angles of the lower limb joints on the sagittal plane, highlighting for the hip: the value at initial contact (H1), the minimum and maximum flexion values (H2 and H3), for the knee, is highlighted the angle at the initial contact and the maximum and minimum value of bending during the stance phase and the absolute maximum value of flexion, respectively K1, K2, K3, and K5. Finally, in the ankle angle are identified: A1 angle at initial contact, A2 maximum plantarflexion, and A3 maximum dorsiflexion.

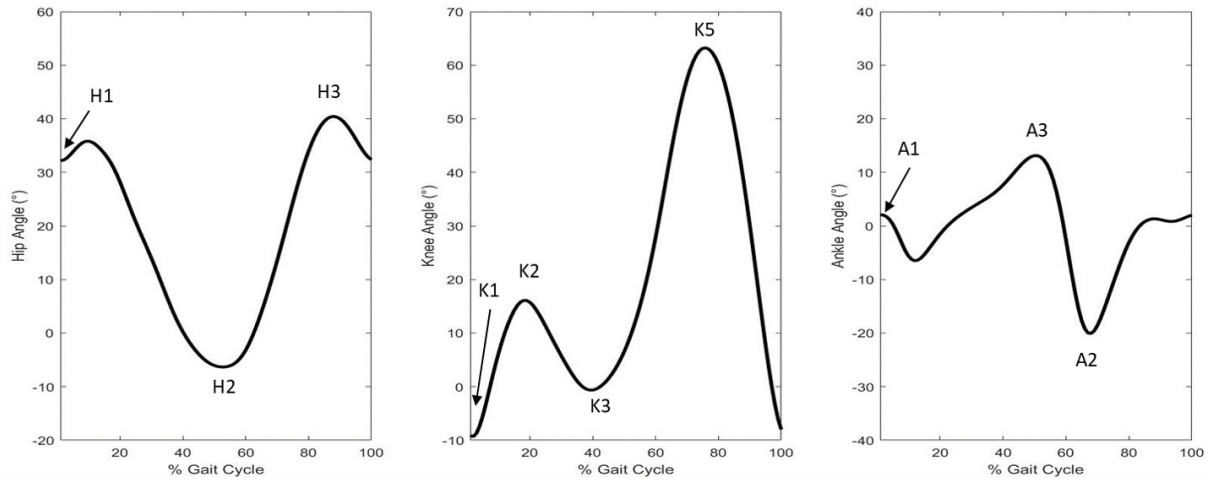


Figure 2.4 - Kinematic curves of the hip, knee, and ankle joint in the sagittal plane and for each of them the main parameters are indicated.

2.3.3 Kinetics Parameters

In addition to kinematic data, kinetic data is also usually derived during gait analysis. We, therefore, speak of kinetic analysis when we investigate the movement taking into account the underlying forces that cause it. The kinetic parameters considered to are the moments and joint forces, these can be obtained through the forces of reaction to the ground (i.e. from the measurements obtained with a force plate) and from the kinematic analysis. Then, by combining it with the subject's kinematic and anthropometric data, such as the subject's height, limb length, etc., a representation of the kinetic data can be determined [5].

Kinetic measurements can be useful for many applications such as the design or evaluation of surgical procedures involving biomechanics or for clinical decision making for patients with pathologies.

Chapter 3

3 Technologies and Systems for Gait Analysis

In this chapter an excursus is made of the main technologies used by laboratories for gait analysis. Since the objective of the thesis lies in comparing traditional tools with novel attractive tracking systems based on machine learning, we take into account the following two technologies: the Vicon, widely considered as the gold standard motion capture system, and OpenPose an open-source, markerless, pose estimation framework that enables, the tracking of the main points of the human body during static and motor activities using deep-learning techniques and videos captured with standard RGB cameras.

3.1 State of the art

There are several techniques that allow to evaluate human movement and its alterations. Depending on the type of analysis to be carried out, qualitative or quantitative, different systems or tools are used.

The **qualitative** analysis analyzes and describes the movements as models, can be carried out through the observation of the moving subject by an expert who evaluates any variations from the normal path without requiring too complex equipment. The observation can also be carried out using tools based on video shooting which are then examined frame by frame, also allowing a comparison between different observations. In any case, the qualitative analysis is linked to the perception and experience of the evaluator because it is a subjective and interpretative approach and difficult to replicate.

On the other hand, **quantitative** analysis describes and analyzes the movement in numerical terms and turns out to be an objective, replicable and comparable approach also with regulatory data. To conduct this analysis, evaluation scales and / or acquisition tools and biomechanical models can be used and the difference in judgment is comparable only to the difference in measurement.

The instrumental evaluation turns out to be the most reliable as it enables the evaluation in the three anatomical planes even of the movements imperceptible to the eye of expert clinicians. Moreover, it allows us to obtain precise and reliable measurements, which are independent from the observer. However, it requires specialized personnel for the interpretation of the results as well as a demanding economic, temporal and technical investment.

This type of evaluation makes use of analysis tools that are mainly divided into two macro-categories: optical and non-optical systems.

Among the commercially available non-optical instruments are a number of sensors that can be used to measure kinematic parameters [7]. Among these there are the electrogoniometers that measure the angular movement of the joints, two-dimensional or three-dimensional, both static and not. This instrument is able to convert the rotary motion into electric current in a proportional way, however it may present some evaluation errors due to crosstalk or positioning errors. There are also inertial electromechanical sensors such as accelerometers [8], which are placed on body segments to measure their linear or angular accelerations up to six degrees of freedom. Other tools available are gyroscopes which measure angular velocity or angles of rotation. All these instruments, magnetic, inertial or electromechanical, allow to obtain kinematic parameters with low costs and miniaturized and / or wearable sensors are preferred in order to be easily positioned on parts of the body and avoid being bulky during the movement of the subject under consideration. Precisely because they must be applied directly on the human body, their result depends: on the positioning which can be critical for some patients and on the choice of the area to be investigated.

Dynamometric platforms are used to derive information on the dynamics of movement [9]. They consist of strain gauges or piezoelectric transducers through which it is possible to calculate the reaction force exchanged between the foot and the ground and the pressures applied by the feet. Force plates are constructed to acquire forces along the three global coordinate axes and their respective moments. The test subject is asked to walk over these force plates which are placed on the laboratory grounds.

In addition to the measurement of kinematic and dynamic parameters during gait analysis, neuromuscular activity can be investigated through electromyography [10]. The electromyographic signal (EMG) is generated by the muscles during their contraction, that is the signal due to the sum of the action potentials generated by the motor units that are located within the sample volume. This signal is collected through invasive electrodes (they observe the signal generated by a few motor units) to understand if the observed muscle contracts and if in the case of a lack of strength the problem lies in the muscle tissue or at the neurological level, or through surface electrodes (they observe the signal generated by a dozen motor units) indicating only if the muscle is active or not or for studies on muscle fatigue. For gait analysis, both surface and invasive electromyography can be conducted based on the objective of the examination to be performed.

The optical systems available today are based on motion capture through the use of cameras positioned within the laboratory, markers positioned on the subject and hardware and software systems [11]. We talk about Optoelectronic systems that are based on the principles of stereophotogrammetry whose objective is the 3D reconstruction of the trajectory of the point that moves in space at each instant of time with respect to the reference system of the laboratory. The number of cameras of these systems is linked to the movement to be analyzed and also to the complexity of the biomechanical model used, in fact usually there are up to 4 cameras for unilateral movement, up to 6 for the analysis of

complete movements but in small volumes or multiple cameras for movement in large volumes.

The markers used can be of two types: passive, they are made of plastic material covered with a reflective film, they require additional lighting devices at a certain wavelength, usually in the infrared, they are spherical and this guarantees wide angles of reflection and they also require preprocessing to identify and classify them. Or they can be active, in this case they are LEDs that generate a light signal, so you do not need an external lighting device and a preprocessing, but they need power supply and synchronization via cable. For the positioning of the markers there are protocols to follow (for example: Davis-Gage, Plug In Gait etc.).

The characteristics of these systems are remarkable as the accuracy of the measurement is high, they are precise and with high resolution and are able to capture the movement in a complete way. However, the errors that can derive from their use are based on instrumental errors, errors in the determination of the coordinates, errors from tissue artifacts or occlusion of some markers perhaps due to the passage of the limbs in front of the markers during the various movements, but they can be intercepted and corrected through support software. The disadvantages are the high cost, the need for large spaces to use them, the setup and calibration that must be carried out before each test which require time and finally the application of the markers because despite the existence of protocols it is very difficult and it needs an expert to do it. Common systems of this type used in movement analysis laboratories are Vicon, Optitrack, BTS etc.

A new category of optical technologies is emerging that today is more used for research purposes and is based on dedicated algorithms to follow the movement of parts of the body. These Tracking algorithms reconstruct the movement of images or videos acquired using mainly RGB cameras and are based on Computer Vision and Machine Learning techniques. There are both devices (like Microsoft Kinect etc.) and licensed or OpenSource software (for example Denspose [12], Openpose [13], Nuitrack [14] ect.). In general, they have a low cost as they were developed for gaming applications but they can be used also for different applications, being not invasive, simple to use , since they do not require calibration or the use of markers, and portable. On the other hand, they are generalized tools and often not suitable for applications that require high-accuracy tracking, they may have occlusion problems and are still considered not mature enough for clinical use.

3.2 VICON

Vicon Motion Capture System is considered the gold standard system of motion analysis laboratories. In fact, it is the most precise, accurate and customizable mocap solution available on the market today. Vicon's optical solutions are used in a wide range of clinical applications, not only for gait analysis but also for the rehabilitation of people with amputated limbs and throughout the field of research that focuses on neurological and motor diseases. In addition, it is the only device that offers a dedicated software platform for acquiring and processing data that allows the integration of other devices such as force

plates or EMG sensors, to conduct the most complete analysis possible. It also allows the possibility of system integration with the most common software such as MATLAB [15], Visual3d, Python, etc.

As previously explained, the disadvantages mainly concern the long acquisition times, the expansive cost, the difficulty in correctly positioning the markers, the possible movement artifacts that derive from their position on the human body and the need to have a large space to carry out the analysis.

3.2.1 Hardware components

Active Wand

It is the dynamic calibration device of Vicon technology (Figure 3.1). It is composed of active markers (LEDs) that allow the calibration on several planes of an entire volume of the optical cameras and of the additional ones for video recording, in addition it has an integrated photodiode to automatically synchronize the wand with the cameras and adjust the brightness of the active markers of the instrument [16]. So for the dynamic calibration of the cameras you have to use this wand that once turned on the LEDs start flashing, when the brightness stabilizes it means that the cameras and the wand are synchronized and then you have to shake the calibration tool in all the volume you want to use for the analysis and the software will then indicate when the calibration has finished effectively.



Figure 3.1 - Active Vicon Wand [16].

Markers

The system is able to work with both the two types of markers previously mentioned: active and passive. For this thesis work, however, only passive markers were used (Figure 3.2) which are also the ones most used in general for rehabilitation applications. These types of markers are retroreflective, they reflect light when illuminated in the infrared, so they

require ad hoc cameras and a light source. Furthermore, in this case they were positioned accordingly to the Plug In Gait protocol for the lower limbs, making sure that they were not too close to each other as they could cause the union of reflexes and therefore errors in data acquisition.



Figure 3.2 - Example of passive markers .

Cameras

For this work, two different types of cameras were used. The first are infrared, since passive markers are used, positioned around the acquisition volume. There were about ten cameras available and they were all used in order to always be sure to intercept all the trajectories of the markers in a precise and accurate way, avoiding occlusions. The cameras are positioned at the top on fixed and immobile supports because even the slightest movement can affect the result of the analysis. Obviously, infrared cameras must first be calibrated and focused.

The other cameras used are of the standard type which have the sole purpose of acquiring and recording the movement during each test carried out to allow to do an analysis based on the observation of the movement of the subjects. Bonita cameras were used for the Vicon system.

Figure 3.3 shows the position of the cameras around the acquisition volume of the Motion Analysis Lab at Spaulding Rehabilitation Hospital in Boston, the positions of the infrared cameras are highlighted with a blue dot and the position of the Standard cameras with a red dot.

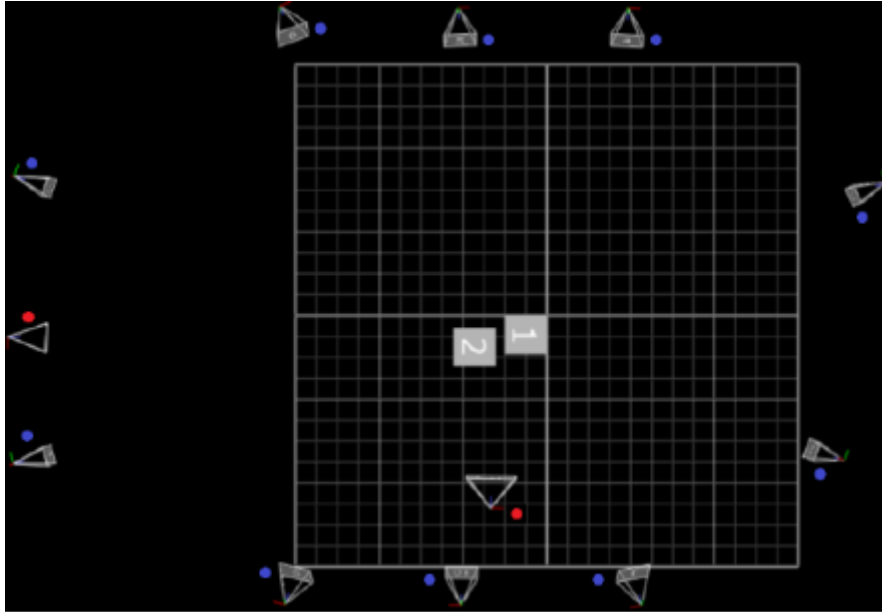


Figure 3.3 - Location of Vicon cameras used in the laboratory and volume of motion they consider.

3.2.2 Software and processing steps

Vicon Nexus software [17] is used to analyze and obtain output data acquired with the mocap system. The software automatically creates and labels a 3-dimensional skeleton for all tests by considering the set of markers used and the characteristic parameters of the subject under examination, such as height, weight, and length of the body segments.

Then, through the predefined biomechanical model chosen within the software, the kinematic and/or kinetic parameters of interest, the names of the markers used, and the relationships between them are extracted.

Figure 3.4 shows the labeling of the markers used and their connection obtained using the Vicon Plug in Gait model for the lower limbs [18].

Obviously, a static test is first carried out where the subject is immobile, with the markers already positioned on the body, at the center of the volume of movement considered by the cameras so that the system can collect all the data on the markers used. After the static test, the dynamic test is carried out which, in this work, consists in walking on the treadmill at different speeds. Once processing procedure is applied to the collected data, it is possible to verify that the acquisition is successful, if there are errors in the identification of the markers or body segments and, if necessary, correct them manually immediately before extracting the parameters of interest

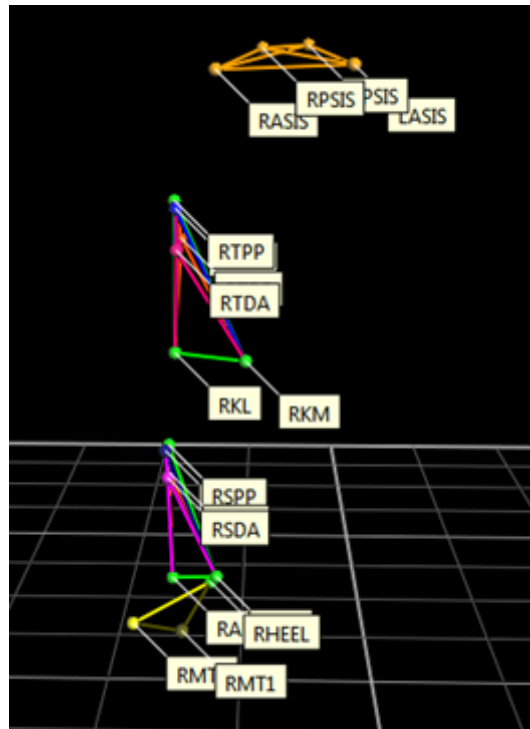


Figure 3.4 - Marker structure and labels on Vicon Nexus.

The model considers six degrees of freedom (DOF) and calculates the outputs in all anatomical planes.

In this work, Vicon Nexus software was used to reconstruct the trajectories of the markers that were later used in the Visual3D software [19], which is a Microsoft Windows application, to extract the kinetic and kinematic data that allows a more robust biomechanical analysis.

Figure 3.5 shows the 6 DOF skeleton on Visual 3D.



Figure 3.5 - Visual3D picture.

3.3 OPENPOSE

OpenPose is a two-dimensional multi-human pose estimation tool. It is based on the use of a parametric representation, Part Affinity Fields (PAFs), that consists in the use of a set of two-dimensional vector fields to identify in the images the parts of the body of all the individuals present [13].

It is important to underline the fact that OpenPose, to identify the main parts of the body, uses a bottom-up approach, i.e., it first recognizes these parts and then associates them with an unknown number of subjects, thus allowing to obtain more accurate results in a less time.

The great advantage lies in the fact that this tool is open-source, real-time, and allows to detect of multiple individuals in a single image even if they are overlapped. It doesn't only focus on tracing the human pose but also the key anatomical points of both the whole body and body districts (hand, foot, and face).

3.3.1 The overall pipeline of OpenPose

The input is an RGB image. The multi-stage Convolutional Neural Networks (CNN) architecture first predicts the set of PAFs, 2D vector fields (L), and detection confidence maps (S) that indicate the belief that a particular body part can be located in a given pixel [13]. Figure 3.6 shows the pipeline followed.

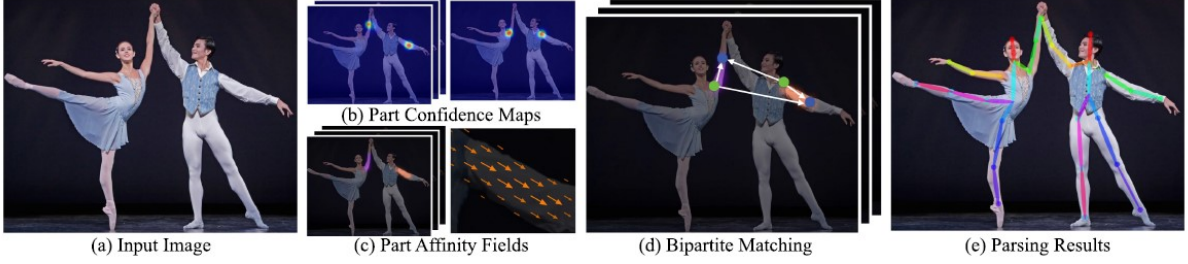


Figure 3.6 - Overall pipeline of OpenPose method [13].

Within the network (Figure 3.7) three consecutive kernels of 3×3 size are used to increase the depth of the neural network.

$$L = (L_1, L_2, \dots, L_C) \text{ where } L_c \in R^{w \times h} \text{ and } c \in \{1, \dots, C\} \quad (3.1)$$

$$S = (S_1, S_2, \dots, S_J) \text{ where } S_j \in R^{w \times h} \text{ } j \in \{1, \dots, J\} \quad (3.2)$$

Hence S has J confidence maps and L has C vector fields for each segment. h and w are the size of the input image.

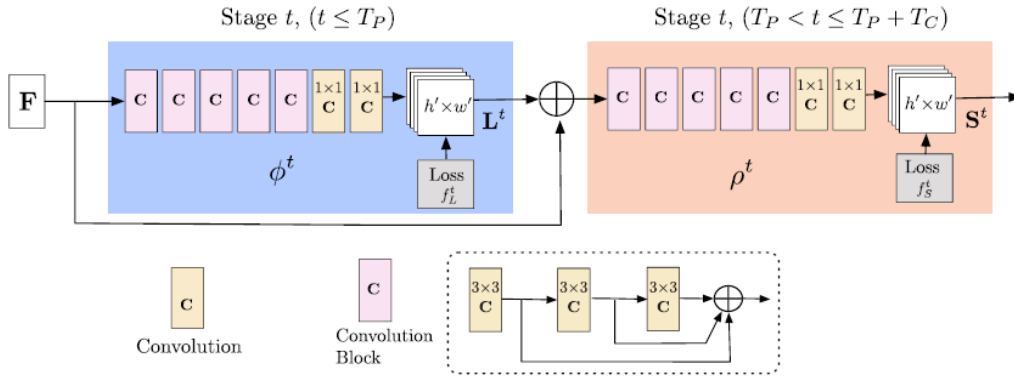


Figure 3.7 - Multi-stage Convolutional Neural Network architecture [13].

Then the image is analyzed by the CNN network and produces F which are a series of functional maps of the image.

In the first stage it produces a series of affinity fields:

$$L^1 = \phi^1(F) \quad (3.3)$$

where ϕ^1 refers to the stage one of CNN interference.

In each subsequent phase (called stage t) both the characteristics F of the original image and the forecasts of the previous phase are concatenated and used for subsequent forecasts:

$$L^t = \phi^t(F, L^{t-1}), \quad \forall 2 \leq t \leq T_p \quad (3.4)$$

where ϕ^t refers to the CNNs for interference at stage t and T_p is the total number of iterations for PAFs.

After all the iterations, everything is repeated to detect the confidence maps S starting from the updated L .

$$S^{T_p} = \rho^t(F, L^{T_p}), \quad \forall t = T_p \quad (3.5)$$

$$S^t = \rho^t(F, L^{T_p}, S^{t-1}), \quad \forall T_p < t \leq T_p + T_C \quad (3.6)$$

Where ρ^t denotes to the CNNs for interference at stage t and T_C is the total number of iterations for confidence maps.

Only the PAFs in each branch are perfected because these produce better confidence maps and, on the other hand, refine the confidence maps has no effect on the PAFs, furthermore, in doing so, the computational time is reduced. Loss functions are applied at the end of each stage which serve to guide the network to predict L and S in an iterative way and so that the network is trained to generate the best L and S .

The loss functions at t_i and t_k stages are:

$$f_L^{t_i} = \sum_{c=1}^C \sum_p W(p) \cdot \|L_c^{t_i}(p) - L_c^*(p)\|_2^2 \quad (3.7)$$

$$f_S^{t_k} = \sum_{j=1}^J \sum_p W(p) \cdot \|S_j^{t_k}(p) - S_j^*(p)\|_2^2 \quad (3.8)$$

The overall loss function combines the previous two to achieve the general objective and is:

$$f = \sum_{t=1}^{T_p} f_L^t + \sum_{t=T_p+1}^{T_p+T_C} f_S^t \quad (3.9)$$

Where p represents the single pixel of the image, S^* and L^* are respectively the fundamental truth confidence maps and the fundamental truth affinity fields. $S(p)$ is a one-dimensional vector that gives me the confidence score of the j th body part in the pixel p of the image. $L(p)$ is the two-dimensional directional vector of segment c in position p . The loss factors are weighted through $W(p)$ which is a binary mask used in order not to penalize the true predictions during training.

Once the parts of the body have been obtained, they must be assembled to form the poses of an indefinite number of subjects and is done through the affinity fields because they have information on both the position of the orientation of the identified segments. Through the PAFs, connections are also provided between the different parts of the body that belong to the same individual in the image.

3.3.2 Use of OpenPose

This tool is released for free and can be used on different platforms (Ubuntu, Windows, Mac OSX), and with different hardware (CUDA GPU, OpenCL GPU, and CPU-only devices). After the installation procedure, it is possible to set up the framework with different settings, such as the input source (e.g., images, videos, or webcams) or the pre-trained model to use for the pose estimation (e.g., body and feet, body only, hands or face). As for the body or body-feet model, one can choose different configurations of the key points of the body and their connection. Currently, 2 models are available in the framework: the COCO MPI model (faster but less accurate) and the BODY 25 model. Figure 3.8 shows the different models. This last model was used for this thesis work because it is more accurate offered by OpenPose at the time of this analysis (Figure 3.9).

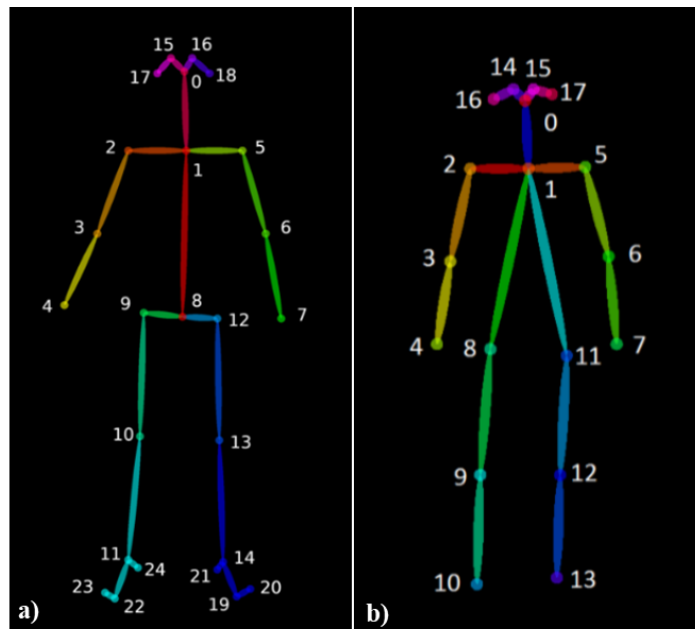


Figure 3.8 - OpenPose Body Model: a) BODY-25, b) COCO [13].

Basically, after acquiring the videos of interest, they are examined through OpenPose which outputs a JSON file for each frame of the video containing the two-dimensional coordinates of each key-point identified and the respective confidence value, index of the algorithm's certain point of the body is found in that precise pixel.

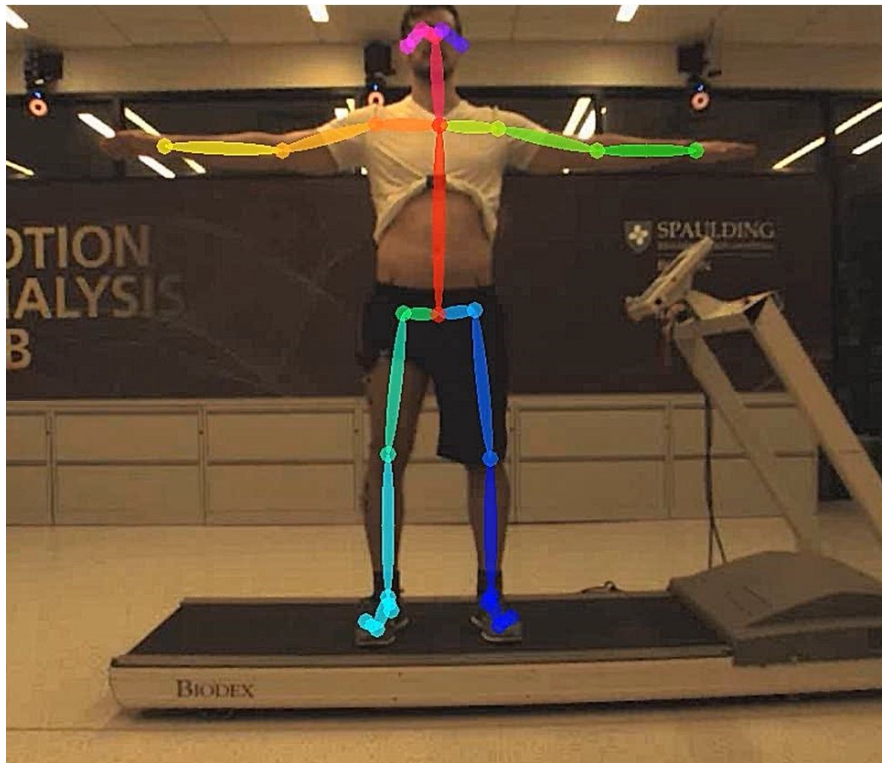


Figure 3.9 - Example of a frame from the static test video taken on one of the subjects examined with the skeleton extracted using OpenPose estimation tool.

Chapter 4

4 Materials and Methods

4.1 Protocol

This paragraph explains the protocol used for data acquisition that was carried out by the Motion Analysis Lab in Boston. In order to make a comparison between the two systems referred to this work, five healthy subjects who did not have any motor problems were recruited. General information regarding these subjects is explained in Table 4.1.

Table 4.1 - Subjects general information.

Subject	Weight (kg)	Height (m)	Age	Gender
1	53	1.67	25	F
2	65	1.80	26	M
3	80	1.70	25	F
4	60	1.71	24	M
5	80	1.83	34	M

20 passive retro-reflective markers were applied to the body of each subject, referring to the Plug-In Gait protocol during their placement.

The position of the markers-set, used for the Vicon system, is defined in this way:

- 1 marker on the C7 vertebra,
- 4 markers on the pelvis of the subject, including 2 in the posterior superior iliac spine for the posterior pelvis and 2 markers in the anterior superior iliac spine,
- 8 markers were used to trace the segments of the right lower limb, 4 of which were positioned to form a square on the thigh and the other 4 to form a square on the leg,
- 2 markers positioned respectively on the medial and lateral epicondyle of the right knee,
- 2 markers positioned respectively on the lateral and medial malleolus of the ankle of the subject's right limb,
- 3 markers were used for the right foot, were placed on the subject's shoe, one of which was placed on the heel, one on the fifth metatarsal, and one on the first metatarsal.

Two other passive markers were placed on the treadmill to calculate its length and to define the new reference system. These markers were positioned:

- 1 marker on the front part of the treadmill,
- 1 marker on the back part of the treadmill.

Two types of trials were performed:

1) Static Trials

It is an important trial that is done for the calibration of the markers but also to define the reference positions. Basically, the subject is asked to stand still and stand on the treadmill in a comfortable upright position.

2) Walking Trials

The subject is asked to walk on the treadmill at three different speeds defined as Fast, Normal, and Slow, randomized in blocks of three. Two acquisitions of about two minutes are made for each speed. So, in the end, are obtained six sessions, two for each speed.

Walking trials are essential for calculating or extracting the angles of the lower limbs during walking but also for determining the position of the joints involved during the GC.

The treadmill was positioned in the center of the volume intercepted by the Vicon system. In addition, the treadmill is used during the data collection in order to obtain the most repeatable walk of the subjects possible and therefore to carry out the tests even in a fixed position, for all subjects, within the laboratory.

During each test the subject was filmed by Vicon cameras, that captured the light reflected by the markers, but also by two additional Bonita cameras, one positioned frontally and one sagittal to the treadmill and so to the subject, which recorded each session whose videos will be used for the OpenPose system but also to validate the performance of the subject.

The same speed for each subject was used for the walking trials in order to obtain comparable walks. The speeds are defined in Table 4.2.

Table 4.2 - Selected speed for each session of walking trial on the treadmill.

Walking Trial	Speed (km/h)	Speed (m/s)
Fast	6.0	1.7
Normal	4.0	1.1
Slow	2.0	0.6

4.1.1 Data collection procedure

First, the Vicon system is activated, the infrared cameras are checked, the standard cameras are positioned and controlled, and the treadmill is positioned. The reference markers are

applied to the latter and then the system must be calibrated through the use of the active wand.

After the preparation of the subject, the trials are performed, 1 for the static trial where the subject is shot both frontally and laterally and 6 for the walking trial, since two walking sessions are performed for each speed.

The videos of each session are obtained from the two standard cameras in lateral and frontal position and from the Vicon infrared cameras, the data necessary for the Vicon system are collected.

As for the Vicon system data, these are extracted through the use of two software, Vicon Nexus, and Visual 3D. Through this software, the trajectories of the joints of the right limb in the three spatial coordinates and the angles of these joints are obtained. This data will henceforth be referred to as Vicon Data.

Instead, the videos of each trial acquired with the standard cameras are first corrected through the information on the lenses of the Bonita cameras that have been obtained with the Matlab "Camera Calibration" tool [20] and then are processed by the OpenPose system which allows obtaining the trajectories two-dimensional key-points of the body of the subject under examination. The data extracted from OpenPose (OpenPose Data) will then be processed and analyzed with the use of Matlab.

4.1.2 Extracted information

Although each trial was acquired both from the lateral and frontal view, the analysis carried out in this work focuses exclusively on the videos of the lateral (sagittal) view. In fact, the markers used for the Vicon system are applied exclusively to the right limb of the subject which is also the limb best viewed from the lateral view.

So, the gait analysis is performed exclusively on the parameters of the subject's right leg. The markers considered during the walking, both for Vicon and for OpenPose, are:

- Right Hip,
- Right Knee,
- Right Ankle,
- Right Heel,
- Right 5th toe,
- Right 1st toe,
- Neck.

Through the software used to analyze the data collected by Vicon, in addition to the spatial coordinates of the mentioned markers, also the angles concerning the hip, knee, and ankle joints are extracted. As regards the OpenPose tool, the coordinates of the before mentioned key-points are extracted, and, instead, the calculation of the angles is performed through the definition of a simplified biomechanical model.

4.2 Rectification of the video

Matlab's "Camera Calibration" tool enables the estimation the intrinsic, extrinsic, and distortion parameters of the lenses of the standard cameras used.

These parameters allow us to match points of the real world with those of the image captured with a camera.

Extrinsic parameters are defined as those that characterize the position and orientation of the camera's reference system with respect to the global one. The origin is in the optical center of the camera, and the x and y axes define the image plane. These parameters are translation and rotation.

The intrinsic ones are the parameters necessary to correlate the pixels of the image, 2D, with the reference system of the 3D camera and are the focal length, the optical center (also called principal point), and the skew coefficient [20].

Then the points of the world are transformed into the coordinates of the camera using the extrinsic parameters and then the coordinates of the camera are mapped in the image plane using the intrinsic parameters (Figure 4.1).

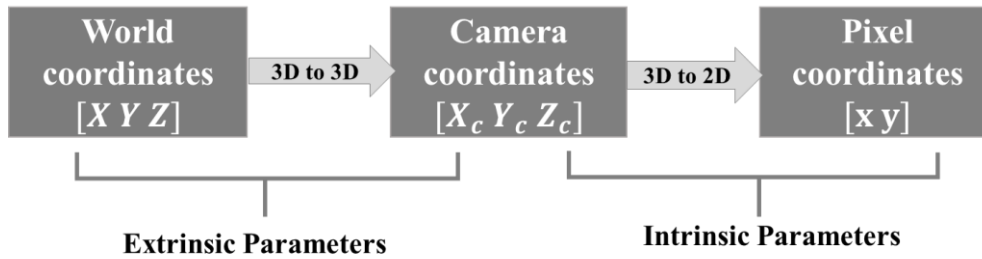


Figure 4.1 - Explanation of the role of intrinsic and extrinsic parameters.

The relationships that allow this are:

$$w[x \ y \ 1] = [X \ Y \ Z \ 1] P \quad (4.1)$$

$$P = \begin{bmatrix} R \\ t \end{bmatrix} K \quad (4.2)$$

$$K = \begin{bmatrix} f_x & 0 & 0 \\ s & f_y & 0 \\ c_x & c_y & 1 \end{bmatrix} \quad (4.3)$$

Where w is the scale factor, x and y the points of the image, and X, Y, Z those of the world. P is the chamber matrix, R and t are the extrinsic parameters, rotation and translation respectively.

K is the matrix of intrinsic parameters and contains $[c_x \ c_y]$ that is optical center in pixels, (f_x, f_y) focal length in pixels that are obtained through:

$$f_x = \frac{F}{p_x}, f_y = \frac{F}{p_y} \quad (4.4)$$

where F is the focal length in the world unit (usually mm) and (p_x, p_y) are the size of the pixel in the world unit. s is the skew coefficient.

A checkerboard with a square size of 23 mm was used as a calibration tool.

The Matlab tool is given as input 43 images (Figure 4.2) that show the chessboard in different positions with respect to the camera, the tool detects the chessboard in each image and then the tool can be calibrated to calculate the parameters of the lenses. It also allows us to extract the final parameters of the lenses and the matrices necessary to eliminate the distortions of each frame of the recorded videos. The lens parameters obtained through this tool are listed in Table 4.3.

Figure 4.3 shows the workflow for getting the corrected videos. In Figure 4.4 you can see the comparison between a frame of one video before and after the rectification.



Figure 4.2 - Example of used input-image with the chessboard.

After obtaining the parameters of the lenses, the Matlab *undistorImage* function is used to obtain the videos without distortion which will then be input to OpenPose to extract the key-points of interest of the subject's body.

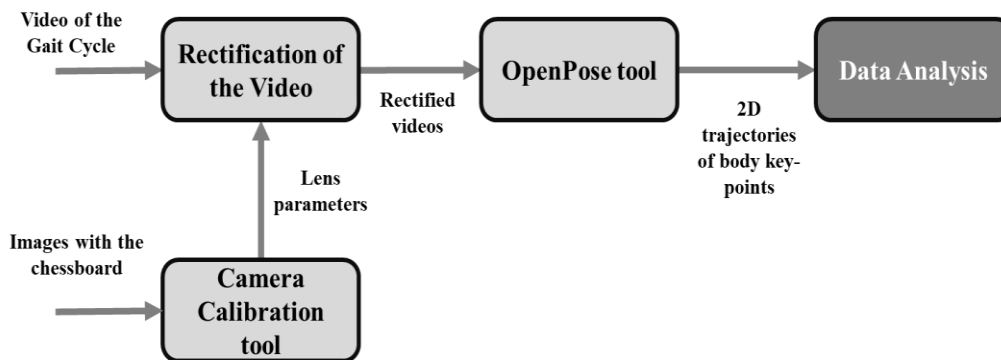


Figure 4.3 - Workflow for video rectification.

Material and Methods

Table 4.3 - Lens Parameters obtained with the camera calibration Matlab tool.

Parameters	
Image Size	[720, 1280]
Radial Distortion	[-0.0494, 0.0017]
Tangential Distortion	[0,0]
World Points	54x2 double
World Units	mm
Principal Point	[634.7126, 359.8283]
Num Patterns	43
Intrinsic Matrix	[336.8044, 0, 0; 0, 334.2413, 0; 634.7126, 359.8283, 1]
Focal Length	[336.8044, 334.2413]
Skew	0
Rotation Vectors	43x3 double
Translational Vectors	43x3 double
Reprojected Points	54x3x43 double
Mean Reprojection error	0.1916
Rotation Matrices	3x3x43 double

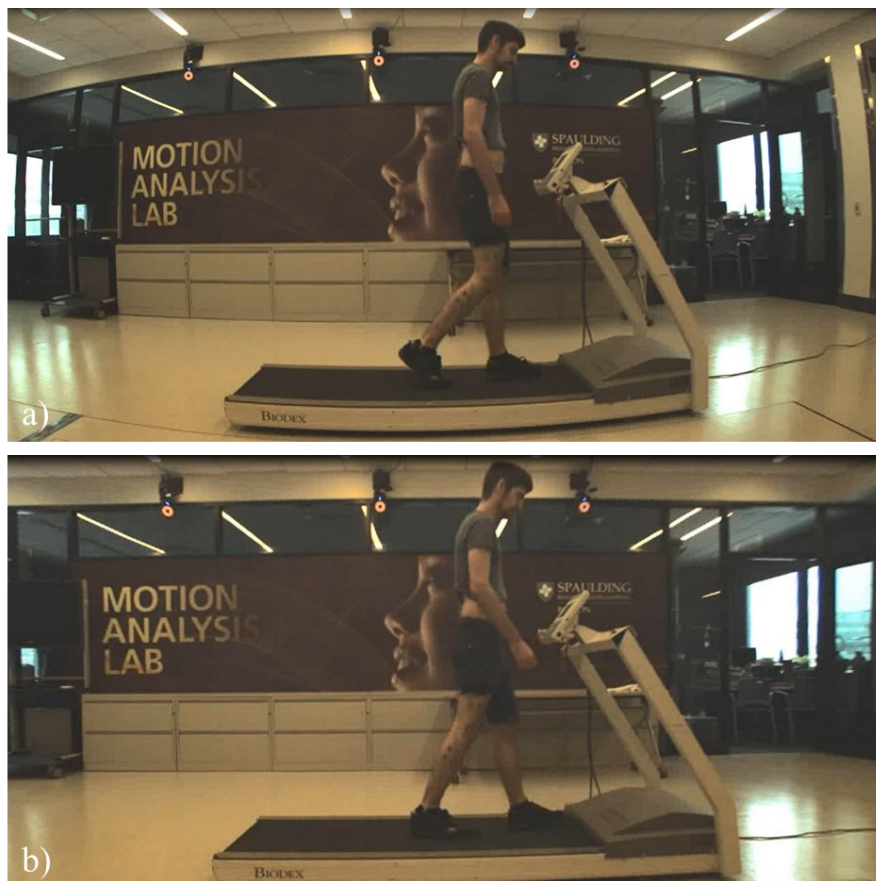


Figure 4.4 - The frame of a video of the walking-trial at Slow speed for Subject 2. In a) the original frame, in b) the rectified frame.

4.3 Data Analysis

To fulfill the purpose of the thesis, after obtaining the Vicon Data and the Openpose Data there is a preliminary analysis part in order to then be able to compare the results obtained with the two systems.

The main steps of this phase (Figure 4.5) concern the definition of a new reference system for both systems, the definition of a conversion factor to pass all the data in the pixel unit, and the processing of OpenPose data. This last step is essential to obtain the comparison, the purpose of the work, between the two systems.

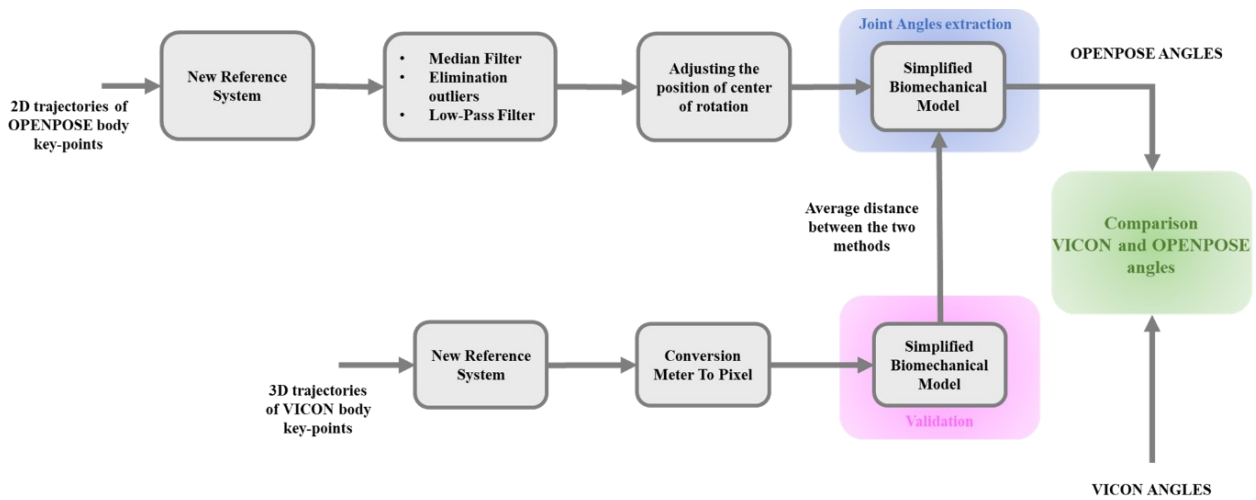


Figure 4.5 - Pipeline of processing data.

In fact, thanks to the processing of OpenPose data, the angles involved by the joints of the lower limb in the sagittal plane are calculated in order to be able to compare them with those already calculated by the gold standard. In addition, the comparison is also based on any difference in the position of the joints traced in each of the systems.

4.3.1 New Reference System

Both systems have their own reference coordinates systems so, in order to perform a comparison, it is necessary to define a common reference system (Figure 4.6). For this purpose, two markers were placed on the treadmill, where the marker positioned in the back is defined with A_1 and the one in the front with A_2 . Point A_2 is chosen as the origin of the new reference system.

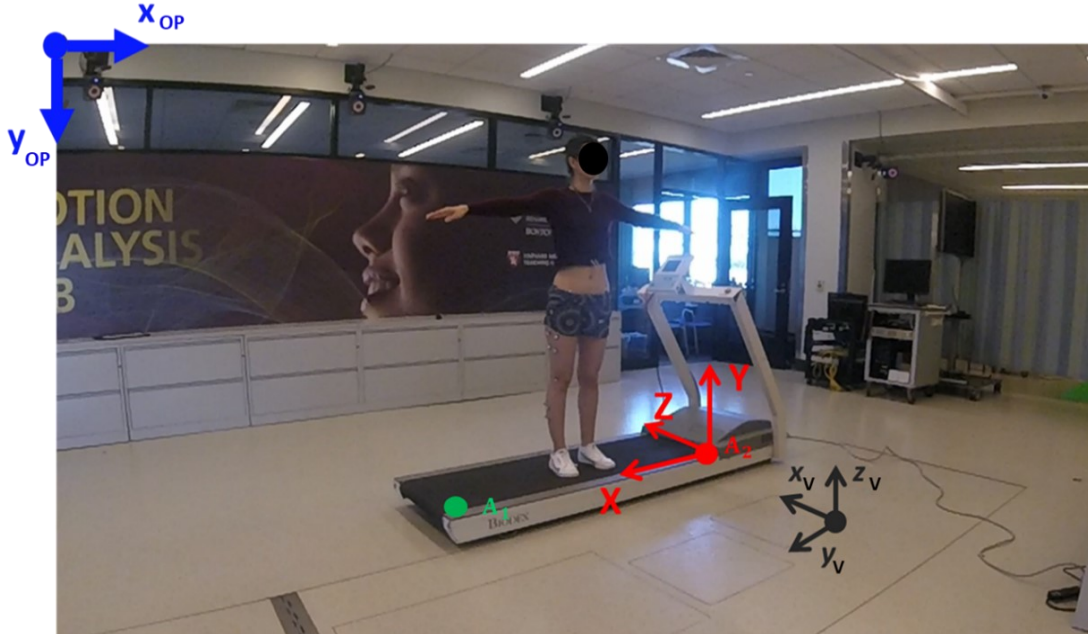


Figure 4.6 - Shows in red the new system of reference that has origin in marker in the front part of the treadmill (A_2), in black the VICON system, in blu the OPENPOSE system in the lateral view and in green the position of the marker in the back part of the treadmill (A_1).

In order to map the data obtained from both Vicon and OpenPose to the new reference system, a transformation operation was carried out. Consider P a generic point, (x, y, z) the new axes of the new reference system, (x_V, y_V, z_V) the axes of the Vicon reference system and (x_{OP}, y_{OP}) the axes of the reference system of OpenPose. Then the coordinates of this generic point with the reference system in A_2 are:

- for Vicon data

$$\begin{cases} P(x) = P(y_V) - \Delta y_V \\ P(y) = P(z_V) - \Delta z_V \\ P(z) = P(x_V) - \Delta x_V \end{cases} \quad (4.5)$$

Where $\Delta x_V, \Delta y_V, \Delta z_V$ represent the distance along the three axes between the Vicon reference system and the new one with A_2 as the origin.

- for OpenPose data

$$\begin{cases} P(x) = -(P(x_{OP}) - \Delta x_{OP}) \\ P(y) = -(P(y_{OP}) - \Delta y_{OP}) \end{cases} \quad (4.6)$$

Where $\Delta x_{OP}, \Delta y_{OP}$ represent the distance along the two axes between the OpenPose reference system in the lateral view and the new one.

4.3.2 Conversion from Meter to Pixel

The results obtained by the two systems are not defined in the same unit of measurement as the Vicon Data are expressed in meters and the OpenPose Data in pixels. Therefore, all the data are converted in pixels through a conversion factor.

As described above, during the data collection, two markers were placed on the treadmill. The conversion was defined based on the length of the treadmill.

The position of these markers was obtained using the Vicon system in its reference system. Instead, the coordinates in the OpenPose reference system were obtained using the Matlab *ginput* function, by selecting manually on the image the points corresponding to the markers positions.

Once the coordinates of the two markers in the two systems were defined, the length of the treadmill l was calculated as:

$$l_{pixel} = \|A_1(y_V) - A_2(y_V), A_1(z_V) - A_2(z_V)\| \quad (4.7)$$

$$l_m = \|A_1(x_{OP}) - A_2(x_{OP}), A_1(y_{OP}) - A_2(y_{OP})\| \quad (4.8)$$

As soon as the treadmill lengths have been obtained in the two units of measurement, the conversion factor (Table 4.4) from meters to pixel is defined as the ratio between the length in pixels and the length in meters:

$$f = \frac{l_{pixel}}{l_m} \quad (4.9).$$

Table 4.4 - Treadmill length in meters and pixels and conversion factor from meters to pixels for all five subjects.

Subject	$l(m)$	$l(pixel)$	Conversion factor
1	1.59	499	312.3
2	1.60	556	347.1
3	1.60	557	348.3
4	1.60	559	348.7
5	1.60	559	348.7

4.3.3 Biomechanical models for computing the angles

In order to carry out the analysis of a subject's gait, the angles associated to the movement of the subject's leg in the lateral view are required. These are: hip angle, knee angle, and ankle angle.

Using the Vicon support software these angles were automatically calculated.

On the other hand, the OpenPose system only gives the coordinates of the key-points of each frame of the video without giving any information about the angles. In this case, a simple biomechanical model was defined to compute the angles with the coordinates extracted from the markerless tracking algorithm.

The joint angles derived by the Vicon software are accurate and rely on a complex biomechanical model which enables the extraction of precise angle measures starting from the 3D coordinates of the markers. In the OpenPose case, only 2D key-points coordinates in the sagittal plane are available and there is no pre-defined biomechanical model. In order to evaluate the impact of the different biomechanical models used in the two systems, a validation procedure is carried out using the same Vicon data as input of the two models. This analysis allows us to quantify the portion of the estimation error related solely to the difference in the biomechanical models, without considering additional variables related to the markerless technology itself (e.g., noisy key-points detection, occlusions, etc.).

The final comparison considers the angles extracted by the original Vicon biomechanical model using the Vicon software and the angles computed using the simplified biomechanical model with the OpenPose key-points coordinates in the sagittal plane. Part of the observed error will be due to the use of different models. Its magnitude can be quantified accordingly to the results of the validation analysis. The details of the methods used to compute the angles in the two biomechanical models are described in the following subsections.

4.3.3.1 Angles definition using the original biomechanical model

Hip angle

The flexion-extension of the hip is calculated around the transverse pelvic axis that passes through the center of the hip joint [18].

Therefore, hip flexion is calculated as the angle between the sagittal axis of the thigh and the sagittal pelvic axis. A positive angle (flexion) value corresponds to the situation in which the knee is in front of the body [18].

Knee angle

Knee flexion is the angle between the sagittal axis of the shank and the sagittal axis of the thigh. It is positive when the knee is flexed.

Ankle angle

Dorsal/plantar flexion is defined as the angle between the axis of the foot and the sagittal axis of the shank. A positive number corresponds to dorsiflexion [18].

Figure 4.7 show the joints, the corresponding movements, and the axes involved in the lower limb in the sagittal plane.

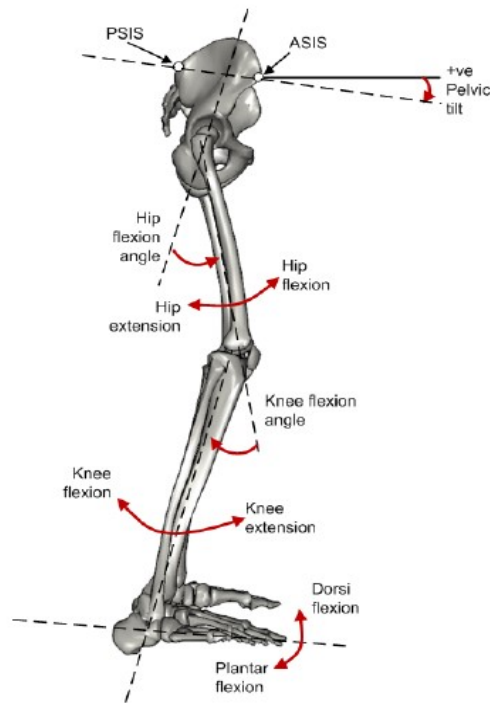


Figure 4.7 - Depiction of the biomechanical definition of the angles of the hip, knee and ankle in the lateral view [18].

4.3.3.2 Angles definition using the simplified biomechanical model

Taking into consideration the way of calculating the angles of the gold standard, a simplified biomechanical model is defined to calculate the angles starting from the coordinates of the key-points of each frame in the sagittal plane for both the Vicon and the OpenPose data.

The method proposed and used for calculating angles using OpenPose data is explained below.

The **hip angle** defined as the angle between the axis perpendicular to the axis of the trunk and the axis of the thigh.

From the lateral point of view, is not possible to have the pelvic axis as there is no depth in OpenPose and also because the key-point of the pelvis center extracted from this instrument is very inaccurate and noisy. Therefore, the trunk axis is not taken into consideration as the one passing through the neck and pelvis center markers but rather as the axis passing through the neck and hip markers.

The thigh axis is defined as the line that intercepts the hip and knee markers.

To define the two axes used to calculate the angle under consideration, the following equations are used:

$$\begin{cases} m = \frac{y_2 - y_1}{x_2 - x_1} \\ k = y_1 - mx_1 \end{cases} \quad (4.10).$$

For the trunk axis, (x_1, y_1) are the coordinates of the neck and (x_2, y_2) the hip coordinates of the frame under consideration.

Using these points and the previous equation, m_1 , and k_1 are defined which are respectively the angular coefficient and known term of the trunk axis. Consequently, the axis perpendicular to the trunk axis has the angular coefficient equal to:

$$m_{1\perp} = \frac{1}{m_1} \quad (4.11)$$

The same is done for the thigh axis, wherein this case m_2 , and k_2 are obtained starting from (x_1, y_1) which in this case are the coordinates of the hip and (x_2, y_2) which are the coordinates of the knee.

So, the angle between the defined axes is:

$$\gamma_{hip} = 90 - \arctan \left\| \frac{m_{1\perp} - m_2}{1 + m_{1\perp} m_2} \right\| \cdot \frac{360}{2\pi} \quad (4.12).$$

As for the knee and ankle angles, these are calculated with the same method used by the gold standard.

For the **knee angle**, the axes of the femur and tibia are defined always using the equation 4.10.

The axis of the thigh considers (x_1, y_1) the coordinates of the hip and (x_2, y_2) the coordinates of the knee of the frame in consideration and using the aforementioned equation we obtain m_1 , angular coefficient, and k_1 , known coefficient.

For the axis of the shank, (x_1, y_1) coordinates of the knee and, (x_2, y_2) coordinates of the ankle, of the frame are considered. Therefore, m_2 and k_2 , angular coefficient, and known coefficient of the tibial segment, are calculated using equation 4.10.

The knee angle is obtained using the following formula:

$$\gamma_{knee} = \arctan \left\| \frac{m_1 - m_2}{1 + m_1 m_2} \right\| \cdot \frac{360}{2\pi} \quad (4.13).$$

The **ankle angle** is calculated using the formula:

$$\gamma_{ankle} = \arctan \left\| \frac{m_1 - m_2}{1 + m_1 m_2} \right\| \cdot \frac{360}{2\pi} \quad (4.14).$$

Where m_1 is the angular coefficient of the leg axis determined using equation 4.10 and the points (x_1, y_1) and (x_2, y_2) which are respectively the coordinates of the knee and ankle. Instead, m_2 represents the angular coefficient of the foot axis found with equation 4.10 through the coordinates (x_1, y_1) and (x_2, y_2) and which represent, respectively, the position of the ankle and the position of the key-point positioned of the first toe (called Medial Toe).

It is important to underline that unlike the common biomechanical models used for calculating the ankle angle, the heel position is not used here only because when extracted from the OpenPose system it was very variable and not very fixed and therefore would have determined errors in the determination of this angle. In fact, preferred to refer to the position of the ankle for determining the axis of the foot in the sagittal plane.

Figure 4.8 shows a schematic of the biomechanical model used and also the axes and key points taken into consideration for determining the angles of the lower limb are shown.

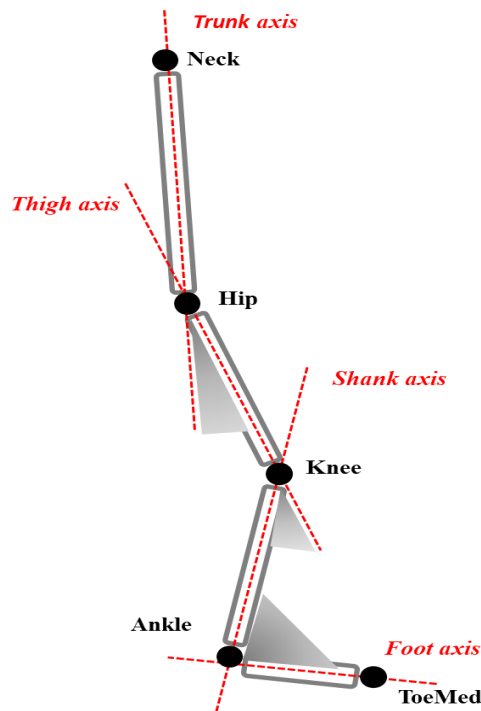


Figure 4.8 - The proposed simplified biomechanical model.

4.3.4 Processing OpenPose Data

After applying the OpenPose algorithm to each video recorded during the walking of each subject, the coordinates, frame by frame, of the body key-points. The trajectories along the two coordinates, x and y , of the points of interest for the gait analysis are noisy and sometimes include outliers. The presence of the outliers means that in that precise frame the tool was not able to determine the correct position of that precise key-point.

In order to solve these problems, filters were applied to the trajectory signals of the key-points.

The first filter applied is a **median filter**. The main purpose of this filter is to remove any outliers present in the signals. A median one-dimensional filter with a positive and odd integer scalar order was chosen, denoted by n . Since the order is odd, it means that the filter returns the median value following the equation:

$$y(k) = x\left(k - \frac{n-1}{2} : k + \frac{n-1}{2}\right) \quad (4.15).$$

The Matlab function used is *medfilt1* and after trying different orders a common value of 5 was chosen for all subjects (Table 4.5).

A **low pass filter** was chosen to remove noise components from the signal. Specifically, an elliptical filter was used as these types of filters meet performance specifications with a lower order than any other type of filter. Since the filter used is an Infinite Impulse Response (IIR) filter, it can have phase distortion, to avoid this an anti-causal filter was used (using the Matlab *filtfilt* function).

The cut-off frequency, f_{cutoff} , (Table 4.5) was chosen through an iterative experimental method. For different frequencies, starting from 1 Hz, the error between the Vicon signal and the OpenPose signal is calculated, and then the frequency that reduces this error is chosen.

Table 4.5 - Shows the values of the window length used for the median filter and the cut-off frequencies chosen, for each subject.

Subject	n	f_{cutoff} (Hz)
1	5	25
2	5	15
3	5	15
4	5	15
5	5	15

Despite the use of the median filter, the trajectories of some subjects still included outliers between the different signal peaks (Figure 4.9) that could not be eliminated with the help of filters without also eliminating the frequency components that were part of the motion signal. Precisely for this reason, a **method for eliminating** these type of **outliers** has been developed. The first derivatives of the signals are computed and the position of the outliers is identified by detecting the peaks in the derivative signal. Once identified, the region around the outliers in the original signal is set to non-valid values. Then, a function based on a autoregressive model is used to fill the artificially created gaps and reconstruct the signal without outliers. Figure 4.10 shows the result obtained on the signals after applying all the techniques explained.

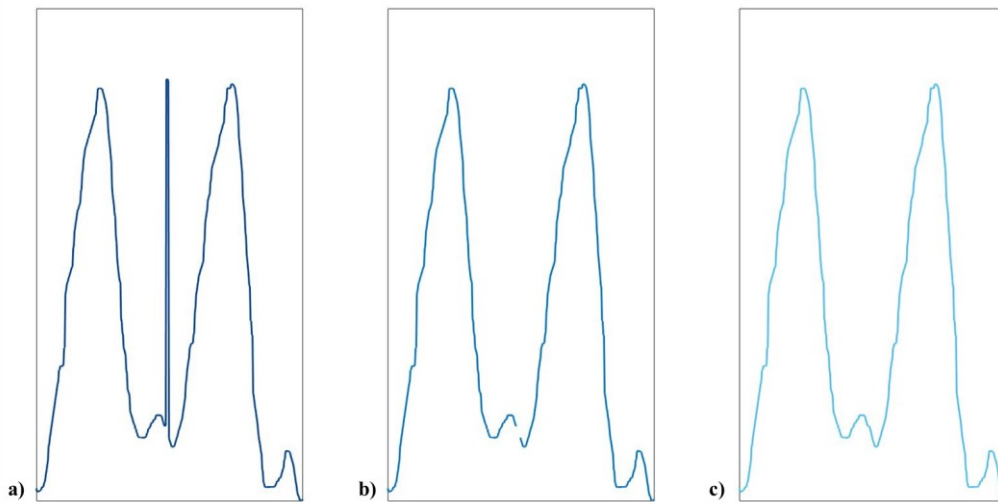


Figure 4.9 - Example of an outlier that persists after using the median filter and how the signal is reconstructed with the method explained. The steps are: a) identification of outliers, b) elimination, c) signal reconstruction. A portion of the X-coordinate signal of subject 4's knee is shown during the first slow speed walking session.

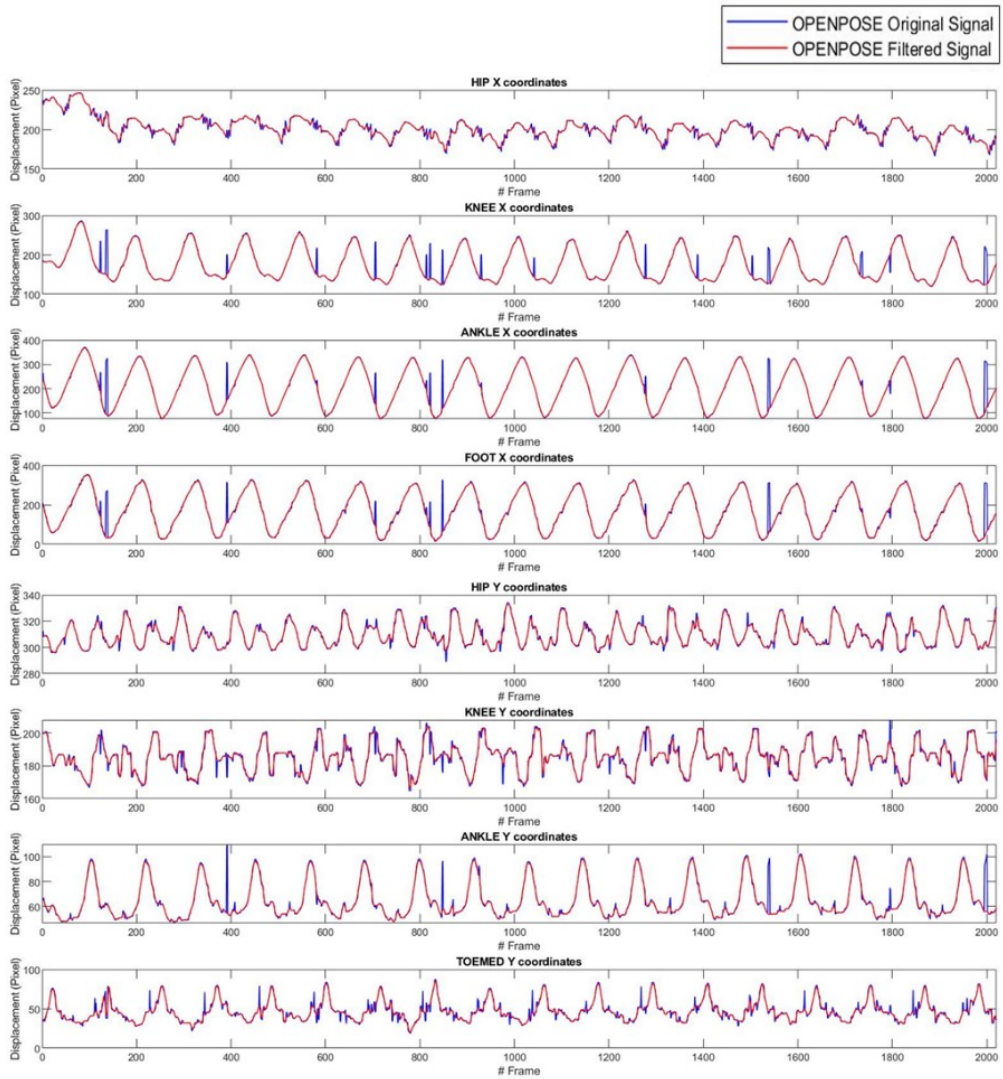


Figure 4.10 - Example of result obtained on signals after filtering them with the median and low pass filter and after applying the outliers removal method. The figure shows the data of the subject 2 in the first Fast speed session.

Chapter 5

5 Results and Discussion

This chapter shows the results obtained from the analysis explained in Chapter 4. These results are also discussed here. Everything focuses on two main aspects: validation of the simplified model used for calculating the angles of the lower limb and comparison of the results obtained using the data extracted in the two systems, Vicon and OpenPose. As far as the comparison is concerned, this focuses on the position of the articular centers of rotation, shape, and amplitude of the angles of the hip, knee, and ankle, and kinematic parameters of the GC.

The results that will be exposed concern the Walking Trials. For each speed, Fast, Normal and Slow, there are two repetitions, of two-minute, that are merged and sampled at 120 Hz. This data is then broken down into GC steps using the Right Heel Strike (RHS) and Right Toe Off events. (RTO). After the subdivision, each step was resampled on one hundred points using linear interpolation in order to represent the data as a percentage of the Gait Cycle.

5.1 Validation of the simplified biomechanical model

The first evaluation concerns the method used to calculate the angles explained in paragraph 4.3.3.2. Validation was carried out to quantify the impact of the use of different biomechanical models for calculating in the two systems.

The validation concerns the use of joint position data extracted with the Vicon system in the proposed simplified model. Then the angles thus obtained are compared with those calculated directly by the Vicon system in order to understand if the method can be considered correct for the subsequent calculation of the OpenPose angles.

For each step, defined through the two events RHS and RTO, the angles are calculated.

Figure 5.1 and Figure 5.3 show the hip, knee, and ankle angles calculated using the Vicon six degrees of freedom model for each walking trial speed for two different subjects. Figure 5.2 and Figure 5.4 show the angles calculated with the method created where the positions of the articular centers extracted from the Vicon system were used as input. The figures

shown refer to two subjects, these have been chosen because they are the most significant for validation.

Once the angles in the two methods described have been obtained they have been compared, as shown in Figure 5.5 and Figure 5.6 where the median of the angles and the corresponding standard deviation of the trend obtained using the different steps available for each subject are represented.

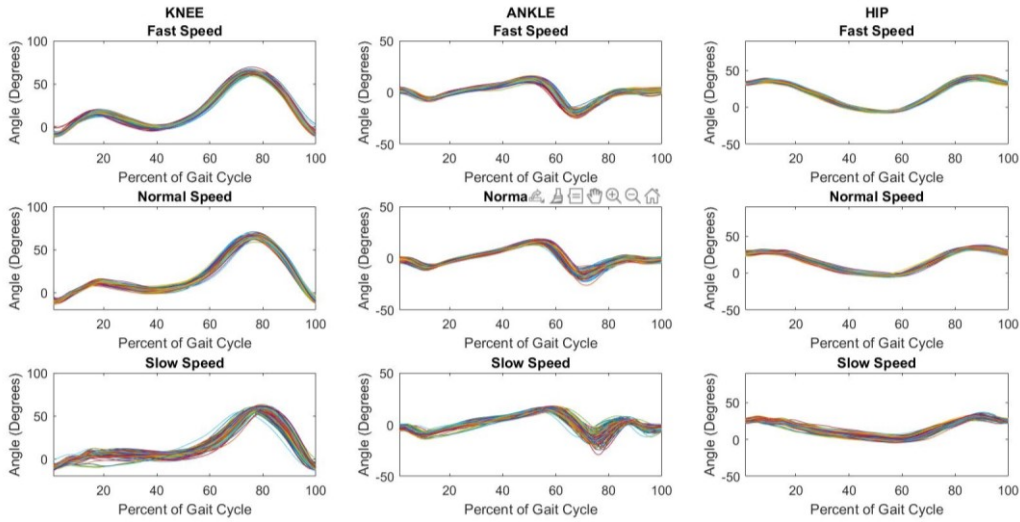


Figure 5.1 - Angles of hip, knee and ankle provided by Vicon system of Subject 1

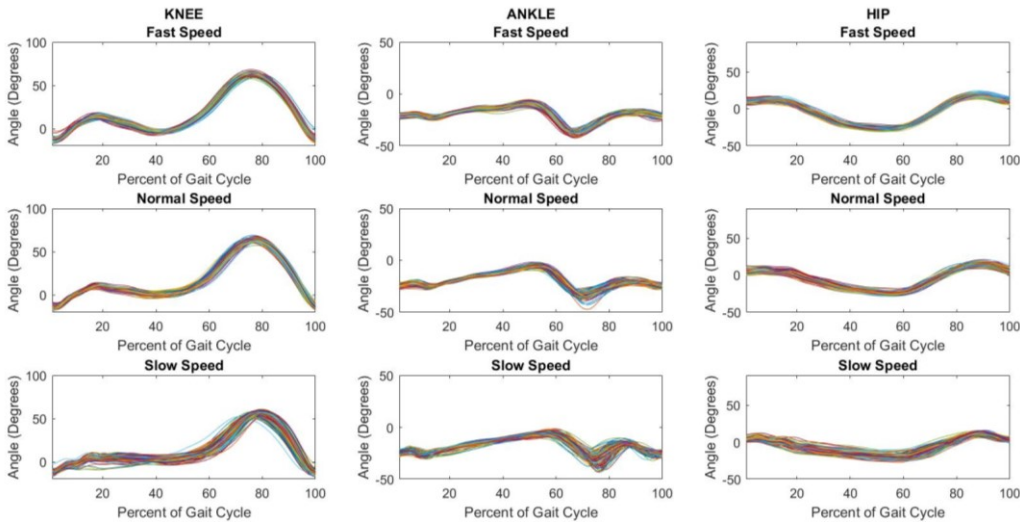


Figure 5.2 - Hip, Knee and Ankle angles extracted with the Proposed Method starting from the position of the joints by Vicon of Subject 1.

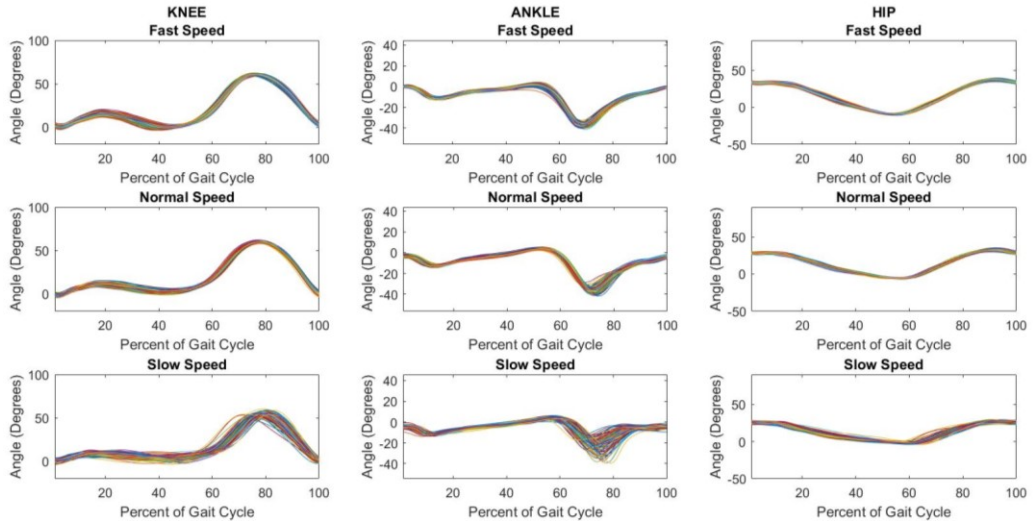


Figure 5.3 - Angles of hip, knee and ankle provided by Vicon system of Subject 5.

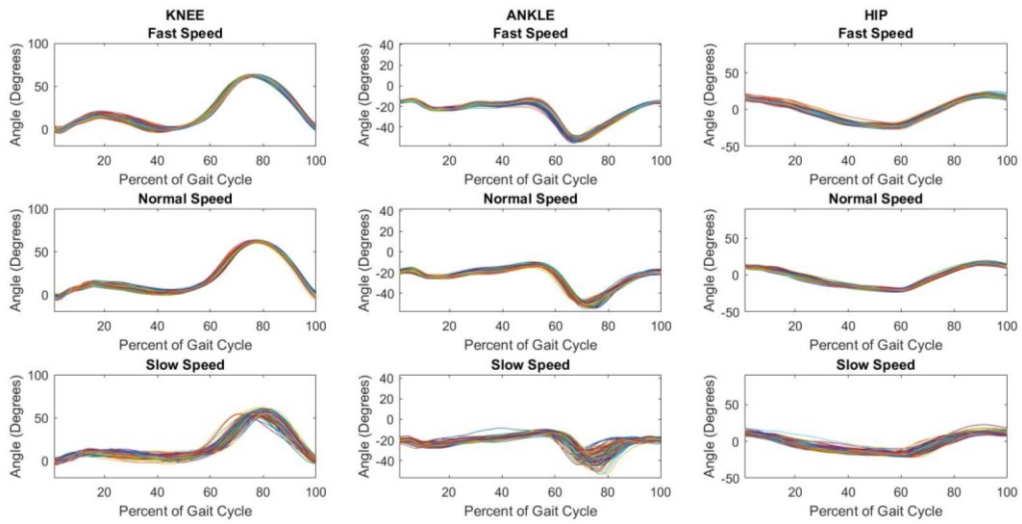


Figure 5.4 - Hip, Knee and Ankle angles extracted with the Proposed Method starting from the position of the joints by Vicon of Subject 5.

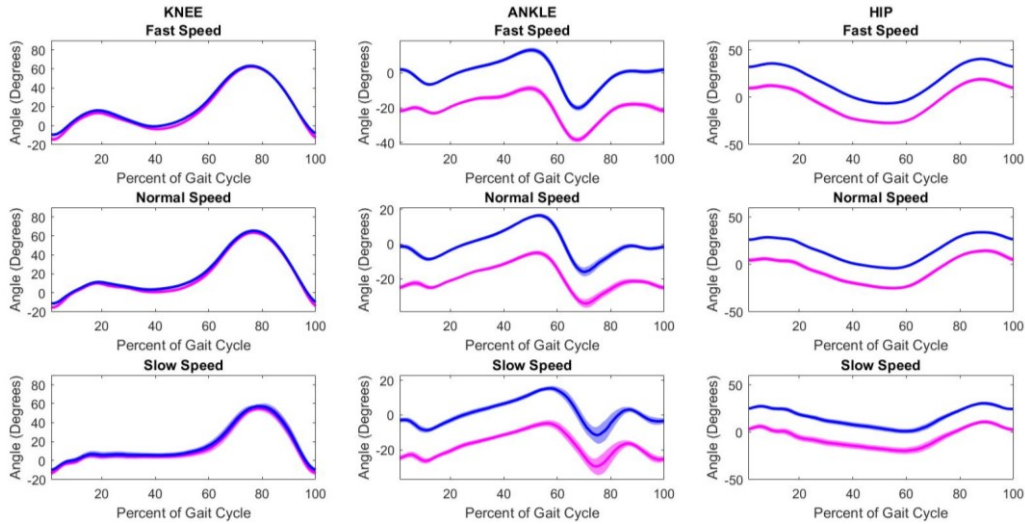


Figure 5.5 - Angles of the Lower Right Limb provided by Vicon, in blue, and angles provided by the Biomechanical model created in this thesis, in magenta (Subject 1).

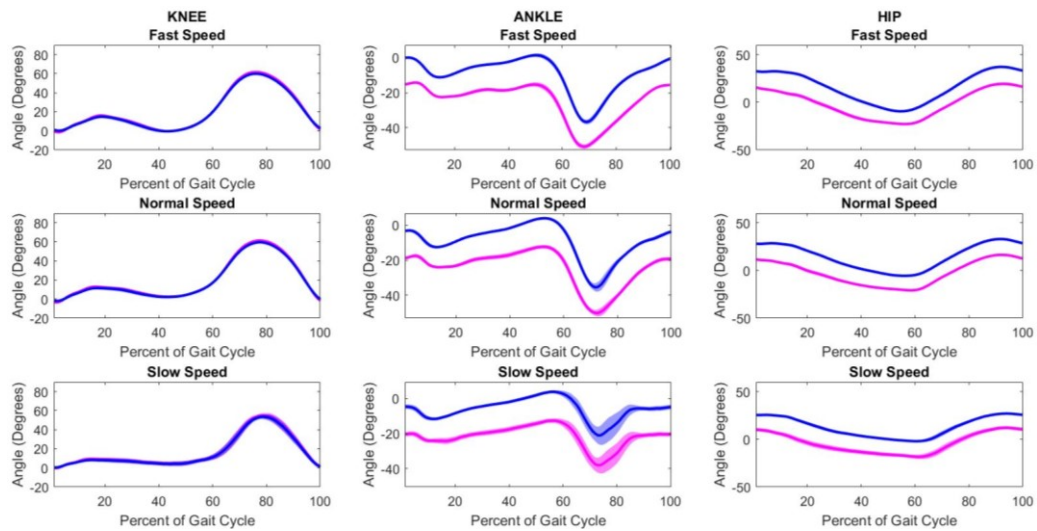


Figure 5.6 - Angles of the Lower Right Limb provided by Vicon, in blue, and angles provided by the Biomechanical model created in this thesis, in magenta (Subject 5).

As you can see in Figure 5.5 and Figure 5.6, there is an underestimation of the ankle and hip angle calculated with the proposed method which is constant throughout the Gait Cycle for both two subjects. This error appears to have a value of about 20 degrees for the hip angle and about 15 degrees for the ankle angle and is present in all subjects. Table 5.1 shows the values of the average distance between the two methods.

Table 5.1 - The average distance for hip angle and ankle angle for all the five subjects.

Average distance between the two methods (°)		
Subjects	Hip angle	Ankle angle
1	21.7	19.4
2	20.5	13.2
3	21.2	10.4
4	17.9	11.0
5	17.3	15.4

These errors were corrected and compensated, obtaining the results in Figure 5.7 and Figure 5.8. In addition to correcting the angles, these errors will also be considered later when calculating the angles with the data of the key-points extracted with the OpenPose system.

After compensating for these errors, statistical values were calculated.

To indicate the discrepancy between the observed data values (Vicon Angle Data) and the estimated data values (Proposed Method), the Root Mean Square Errors (RMSE) was calculated for each step considering all the angles of the entire Gait Cycle.

$$RMSE = \sqrt{\frac{\sum_{i=1}^n (\alpha_1 - \alpha_2)^2}{n}} \quad (5.1)$$

Where α_1 and α_2 are respectively the Vicon angle and the angle calculated with the average created both in the current step.

Figure 5.9 and Figure 5.10 show RMSE calculated for each step and Table 5.2 shows the average RMSE value for each angle and subject examined.

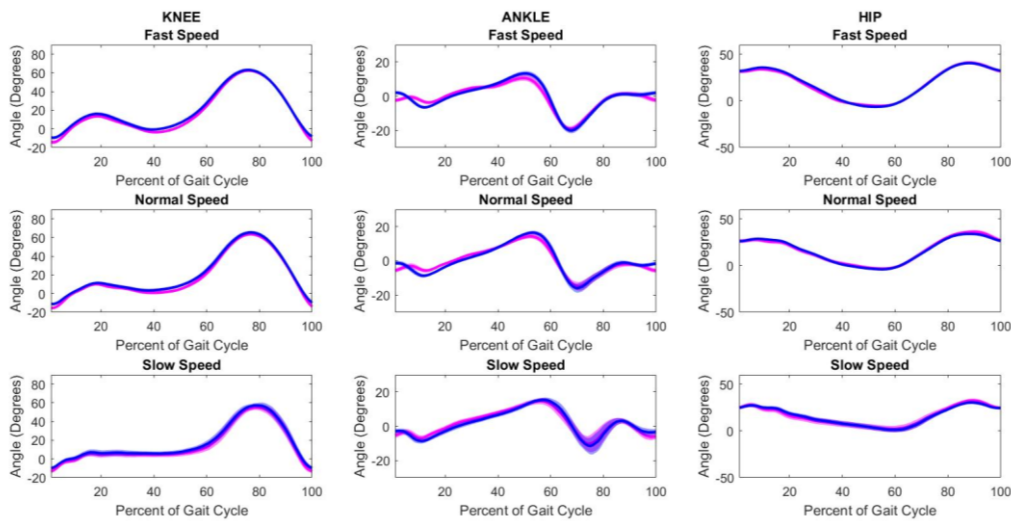


Figure 5.7 - Hip, Knee, and Ankle angles of the Vicon system, in blue, and corrected angles, with the adjusted offset, obtained with the method used in this thesis, in magenta (Subject 1).

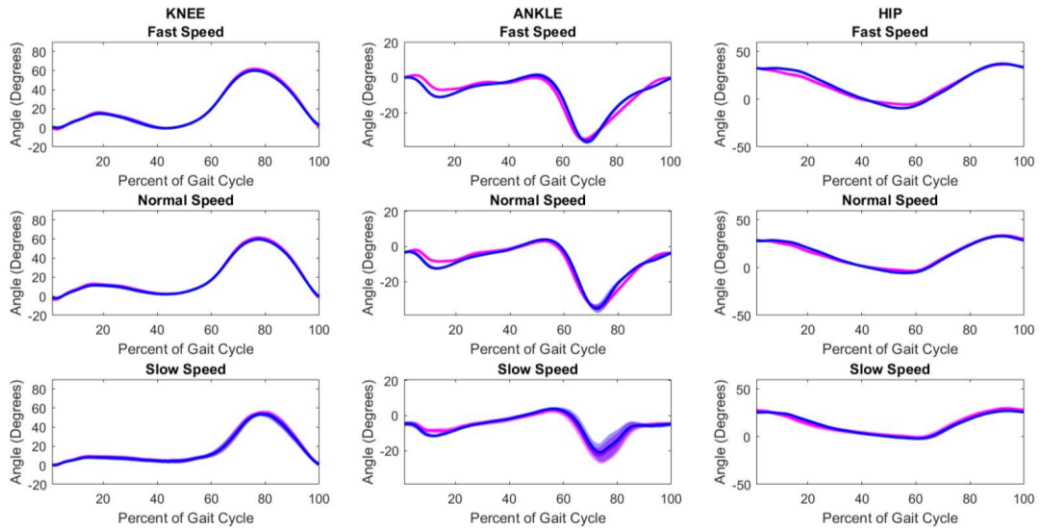


Figure 5.8 - Hip, Knee, and Ankle angles of the Vicon system, in blue, and corrected angles, with the adjusted offset, obtained with the method used in this thesis, in magenta (Subject 5)

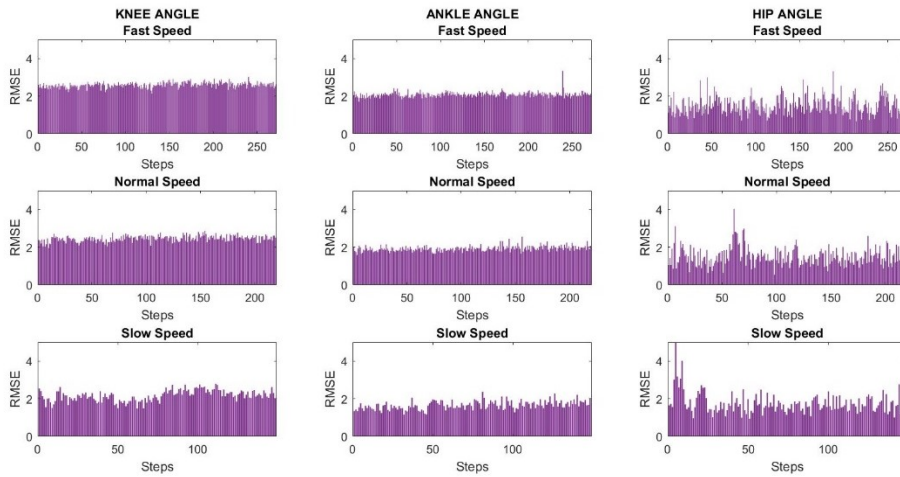


Figure 5.9 - RMSE calculated for each step (Subject 1).

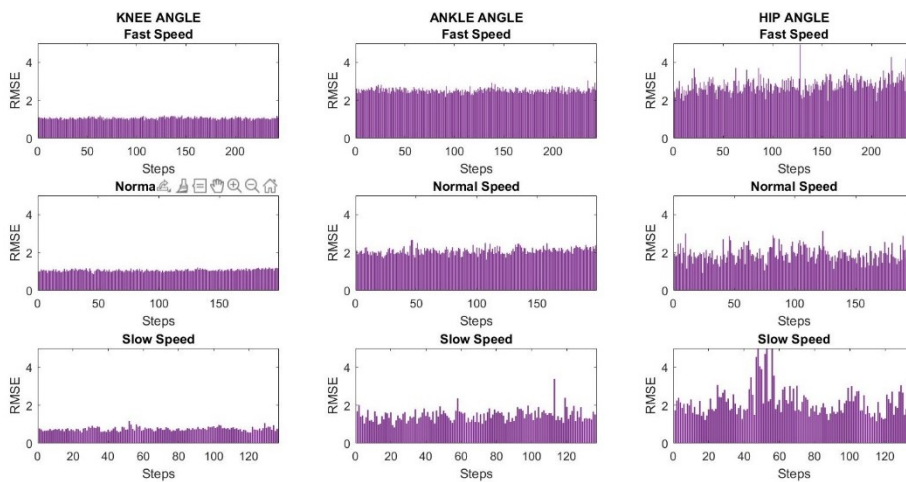


Figure 5.10 - RMSE calculated for each step (Subject 5).

In addition, the Mean Absolute Error (MAE) between the Vicon Angle Data and the calculated angles was calculated using the following formula:

$$MAE = \frac{1}{n} \sum_{i=1}^n \|\alpha_1 - \alpha_2\| \quad (5.2)$$

Where α_1 and α_2 have the same meaning as Equation 5.1. The final value of the MAE, for each angle of each subject, is obtained as the average value of the n steps. Table 5.3 shows the average, maximum, minimum values of the MAE and the corresponding standard deviation.

Table 5.2 - Average RMSE values of the angles of the lower limb for each subject.

		Subjects				
		1	2	3	4	5
Mean	Hip angle	1.57	1.64	3.36	1.27	2.37
RMSE (°)	Knee angle	2.45	1.29	1.29	1.03	0.99
	Ankle angle	1.94	1.34	1.34	1.75	2.13

Table 5.3 - Mean value, standard deviation, maximum and minimum values of the mean absolute error between the Vicon angles and the angles calculated with the created biomechanical model using the coordinates of the joints extracted with the Vicon system.

		Subjects				
		1	2	3	4	5
Hip angle (°)	Mean value	1.33	1.37	3.12	1.05	1.92
	Standard Deviation	0.90	0.92	2.27	0.75	1.00
	Max value	2.49	3.57	4.45	1.98	5.04
	Min value	0.67	0.52	1.19	0.623	0.61
Knee angle (°)	Mean value	2.17	0.98	0.95	0.79	0.78
	Standard Deviation	0.44	0.18	0.38	1.44	0.19
	Max value	4.80	3.21	3.72	3.26	1.96
	Min value	0.24	0.09	0.21	0.09	0.06
Ankle angle (°)	Mean value	1.58	1.09	1.04	1.44	1.66
	Standard Deviation	0.53	0.47	0.61	0.91	0.59
	Max value	4.43	3.30	2.93	3.51	4.75
	Min value	0.36	0.29	0.39	0.19	0.26

As shown in Figure 5.5 and Figure 5.6, it can be noticed that there is a consistent error made by the simplified model in the extraction of the joints angles. The fact that this error is constant along the Gait Cycle for the hip and ankle angles shows how, for these two angles, this error can be compensated. After calculating the average value of this error for each subject, the origin of this discrepancy must be investigated. This error could be the result of changes made in calculating the hip and ankle angle compared to how they are calculated by the gold standard. So, the origin of the error is found in the consideration of the different axes used to calculate these angles. In fact, the angle of the hip was not calculated as the angle between the pelvic axis and the femoral axis as defined by the Vicon system, but rather as the angle between the axis perpendicular to the trunk axis and the axis of the thigh. This change is caused by the inability to correctly observe the key-point of the pelvis center from the lateral view, through the OpenPose system. This could result in the underestimation of the hip angle as is evident from the results obtained in the validation.

As for the angle of the ankle, its underestimation may have resulted from the fact that the model considered the line that passes through the ankle and Medial Toe key-points rather than between the heel and foot key-points was considered as the foot axis. This choice was made consciously, as the consideration of the heel key-point was excluded a priori precisely because the high oscillation that this point had during the walk of the subject was evident from the videos extracted with the OpenPose system.

The compensation of these errors was therefore considered correct as they proved to be constant along the gait cycle of the subjects. In fact, after their correction, the model created was considered to be quite robust because, as seen in Table 5.3, the maximum error between the angles calculated in the two systems never exceeds 5 degrees and the average value is always less than about 3 degrees in all angles and for all subjects.

The RMSE obtained for each subject was also considered acceptable as in the worst case it has a value close to 3 degrees as shown in Table 5.2.

The offsets indicated in Table 5.1 were corrected to allow us to directly compare the angles computed with Vicon and the OpenPose systems, for each subject. Additional data and further analysis will be needed to define a general rule to correct the offset between biomechanical models.

5.2 Joint center position

The comparison is also based on the position of the body joints in the two Motion Analysis systems used in this work. A first analysis is based on the distance between the key-points estimated by the OpenPose system and the rotation centers calculated by the Vicon system. Two metrics were used for this distance-based comparison.

The first metric concerns the definition of Mean Absolute Errors, which was calculated for both the trajectories of the joints along the x-axis and along the y-axis using the following formula:

$$MAE = \begin{cases} \frac{1}{n} \sum_{i=1}^n \|x_V - x_{OP}\| \\ \frac{1}{n} \sum_{i=1}^n \|y_V - y_{OP}\| \end{cases} \quad (5.3)$$

Where x_V and y_V are the positions at the i -th frame of the joint in consideration obtained by the Vicon system and x_{OP} and y_{OP} are the corresponding positions obtained by the OpenPose system. n is the total number of frames.

Therefore, an MAE value is obtained for each subject and for each session of the walking trial. The final value for each subject, shown in Table 5.4, was obtained as the average value of the error of all sessions.

The second metric used is the Euclidean distance between the positions of the joints in the two different systems. The equation used is:

$$distance_{euclidean} = \sqrt{(x_{OP} - x_V)^2 + (y_{OP} - y_V)^2} \quad (5.4)$$

Where (x_V, y_V) and (x_{OP}, y_{OP}) are the coordinates of the joint centers of rotation in the two systems.

Also, in this case, Table 5.5 shows the average values obtained with respect to each session of each subject.

The distances measured with the two metrics are reported in centimeters in order to be understood in a simpler and more intuitive way. The values in centimeters are obtained through the inverse use of the conversion factor defined in Paragraph 4.3.2.

Table 5.4 - Distance, in centimeters, between the OpenPose landmarks and the Vicon joints.

		Subjects				
		1	2	3	4	5
Neck (cm)	X	4.16	1.55	3.02	2.87	2.16
	Y	8.93	11.9	12.8	14.5	13.1
Hip (cm)	X	4.58	2.45	7.01	3.56	3.40
	Y	0.95	1.99	2.96	2.22	2.22
Knee (cm)	X	1.43	2.07	4.91	2.63	1.66
	Y	2.94	4.01	2.78	2.94	3.93
Ankle (cm)	X	1.50	2.33	2.77	2.38	2.01
	Y	3.93	5.86	5.84	5.72	6.45
Medial Toe (cm)	X	1.79	2.73	2.60	2.79	2.54
	Y	4.20	7.53	6.95	7.13	6.87
Lateral Toe (cm)	X	1.35	3.28	3.34	2.79	2.17
	Y	3.97	7.27	5.00	6.87	5.96
Heel (cm)	X	3.28	2.83	1.82	2.40	3.32
	Y	4.08	4.76	2.17	3.60	4.36

An important step that has been applied in this work and which primarily concerns the positions of the articular centers obtained by OpenPose is their repositioning or also defined in Figure 4.4 as 'Adjusting the position of center of rotation'. Basically, the coordinates of the OpenPose joints have been adjusted by compensating for the average absolute error shown in Table 5.4 in such a way as to reposition the joints more or less in correspondence with those of the Vicon system so that the subsequently extracted angles had no errors that could be determined from incorrect alignment of the joints.

Table 5.6 shows the Euclidean distance values between the joints identified in the two systems obtained after this compensation operation.

Table 5.5 -Euclidean distance, in centimeters, of the OpenPose landmarks and the Vicon joints.

	Subjects				
	1	2	3	4	5
Neck (cm)	9.91	12.1	13.3	14.8	13.4
Hip (cm)	4.73	3.53	7.79	4.49	4.36
Knee (cm)	3.43	4.69	5.84	4.18	4.39
Ankle (cm)	4.32	6.52	6.65	6.37	6.89
Medial Toe (cm)	4.77	8.27	7.63	7.95	7.59
Lateral Toe (cm)	4.30	8.22	6.20	7.62	6.55
Heel (cm)	5.59	5.92	3.10	4.74	5.95

As can be seen from Table 5.4, the greatest distances between the key-points obtained by the two systems occur especially, along the Y-axis, for the neck, ankle, and foot markers, and, along the x-axis, for the hip marker. Examples of these distances for one subject are shown in Figure 5.11 and Figure 5.12 where are represented the trajectories along the y axis of the mentioned above markers that have a higher mean absolute error. These trajectories are expressed in the gait cycle and are represented by the median and standard deviation of the trends using the different steps available for the subject.

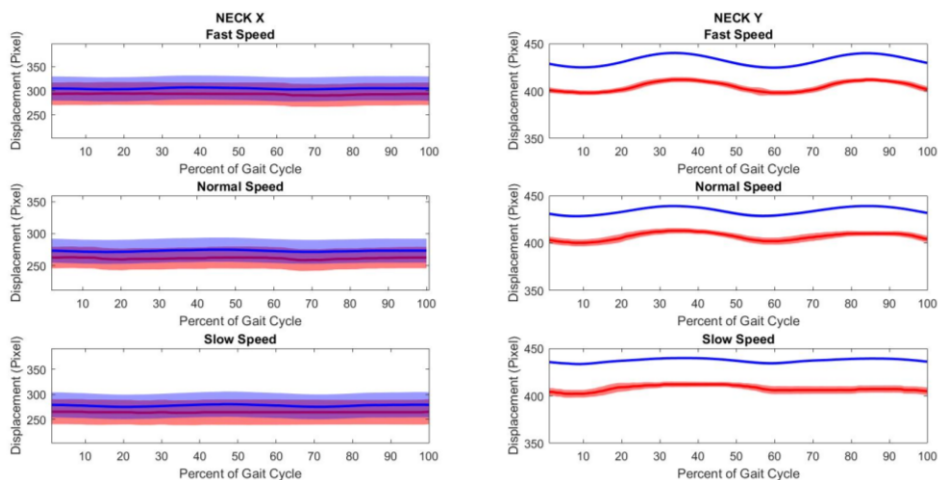


Figure 5.11 - Comparison between Vicon, in blue, and OpenPose, in red, Neck coordinates along x and y axis (Subject 1).

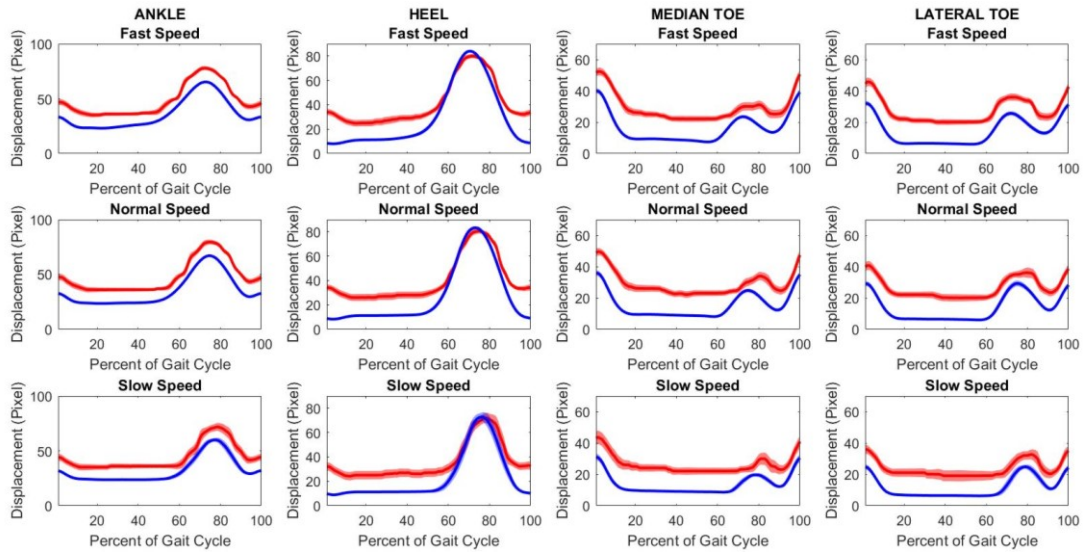


Figure 5.12 - Comparison between the coordinates, along the y-axis of Ankle, Heel, Median Toe and Lateral Toe, Vicon, in blue, and OpenPose, in red. (Subject 1).

Table 5.6 - Euclidean distance after the error compensation.

	Subjects				
	1	2	3	4	5
Neck (cm)	1.23	1.09	2.51	0.89	1.35
Hip (cm)	1.55	2.21	2.44	1.94	1.90
Knee (cm)	1.69	1.56	1.82	1.65	1.53
Ankle (cm)	1.50	2.41	2.08	2.30	2.18
Medial Toe (cm)	2.11	2.92	3.38	3.38	2.71
Lateral Toe (cm)	1.55	2.56	2.51	2.75	2.28
Heel (cm)	2.80	3.47	2.36	3.12	3.23

At a statistical level, the Pearson correlation index is calculated between the trajectory signals of the joints obtained with the gold standard and with the modern system precisely because this index indicates whether there is a linear correlation between the two. The formula for calculating Pearson's coefficient is given by the following equation:

$$P_{coeff} = \begin{cases} \frac{\sigma_{x_V x_{OP}}}{\sigma_{x_V} \sigma_{x_{OP}}} \\ \frac{\sigma_{y_V y_{OP}}}{\sigma_{y_V} \sigma_{y_{OP}}} \end{cases} \quad (5.5)$$

Where in the numerator there are the covariances between the trajectories of the joints obtained by the two systems and in the denominator the product between the two standard deviations. Table 5.7 shows the values obtained for each subject and for each of his body joints.

Table 5.7 - Pearson correlation index between the trajectories of the landmarks, both along the x and y-axis, of the two motion tracking tools.

		Subjects				
		1	2	3	4	5
Neck	X	0,988	0,975	0,792	0,982	0,985
	Y	0,874	0,939	0,750	0,891	0,845
Hip	X	0,975	0,938	0,960	0,940	0,966
	Y	0,868	0,783	0,652	0,650	0,756
Knee	X	0,995	0,995	0,992	0,993	0,998
	Y	0,858	0,918	0,754	0,949	0,874
Ankle	X	0,998	0,994	0,996	0,998	0,999
	Y	0,978	0,976	0,971	0,985	0,932
Medial Toe	X	0,998	0,993	0,995	0,998	0,997
	Y	0,862	0,868	0,783	0,800	0,701
Lateral Toe	X	0,999	0,994	0,996	0,998	0,998
	Y	0,923	0,892	0,780	0,921	0,802
Heel	X	0,997	0,991	0,994	0,995	0,996
	Y	0,972	0,981	0,974	0,975	0,920

The MAE is the first parameter calculated to compare the positions of the reference points estimated by the OpenPose tool and the centers of rotation obtained by the Vicon system.

As can be seen in Table 5.4, the main anatomical points that have the greatest discrepancies are mainly the hip along the x-axis and neck, ankle, and the points referring to the foot along the y axis.

As for the neck key-point, Figure 5.11, this high error along the vertical axis is not correlated with a poor estimate by the OpenPose tool but rather concerns the different definitions of this marker in the two systems. In fact, in Vicon the neck marker is positioned on the C7 vertebra while OpenPose identifies it further down in the middle position between the two shoulders.

The error obtained for the hip marker along the x-axis is an error of the OpenPose tool as it is difficult for it to correctly identify the hip marker precisely because there is a lack of additional information for its localization. Furthermore, during the walk from the lateral point of view, it could happen that the subject had his arms placed sideways along the hips and this caused more an error in the estimate of the hip joint.

Finally, for the ankle and foot markers, Figure 5.12, the greatest error is always on the y-axis, this is because the OpenPose tool identifies them in a position that is elevated with respect to the points identified by the Vicon system. It cannot, therefore, be determined as an error of the modern tool but rather as a different evaluation of those joints.

The calculation of the Euclidean distance and the results obtained in Table 5.5 confirm the considerations already made on the distance between the body points identified by the two systems. Especially regarding the neck marker, it shows how the Euclidean distance is more or less constant and have roughly the same value between all subjects, which also happens for the ankle and foot markers.

Obviously, the results improve especially after the error compensation operation, as shown in Table 5.6. Especially for markers of interest for calculating angles, it is noted that they all have a Euclidean distance of less than 3.5 cm. The fact that, however, despite the error being corrected, the position of the key-points between the two systems is not perfectly equal is because the error was compensated by using an average value.

Table 5.7 shows the Pearson correlation indices between the trajectories of the joints both along the x and y axes of the two tools used.

The Pearson coefficient defines the correlation between the two variables, this is weak when the absolute value of the coefficient is between 0 and 0.3, moderate when it is between 0.3 and 0.7, and strong correlation when it is greater than 0.7.

It can be seen from the results shown in Table 5.7 that there is always a positive and strong correlation, this means that although the OpenPose tool is not very precise and that the trajectories extracted are not always perfect they are still correlated and similar to those obtained with the gold standard.

5.3 Angles of the lower limb

After validating the biomechanical model created to calculate the angles, these were extracted using the coordinates of the joints obtained with the OpenPose system.

Figure 5.13 and Figure 5.14 show the angles of the hip, knee and ankle obtained for the different speeds of the walking trial. The first figure shows the angles obtained directly from the Vicon system; the second shows the articulation angles derived from the coordinates of the key point extracted with the OpenPose system (and therefore the angles calculated with the simplified biomechanical model explained in the paragraph 4.3.3.2). Figure 5.15 and Figure 5.16 show the same data but for another subject. The subjects that have been chosen to represent through the figures are those considered most significant, since they exemplify the different level of noise in the data.

Also, in this case, the angles expressed as a percentage of the Gait Cycle are shown and divided into steps using RHS and RTO events.

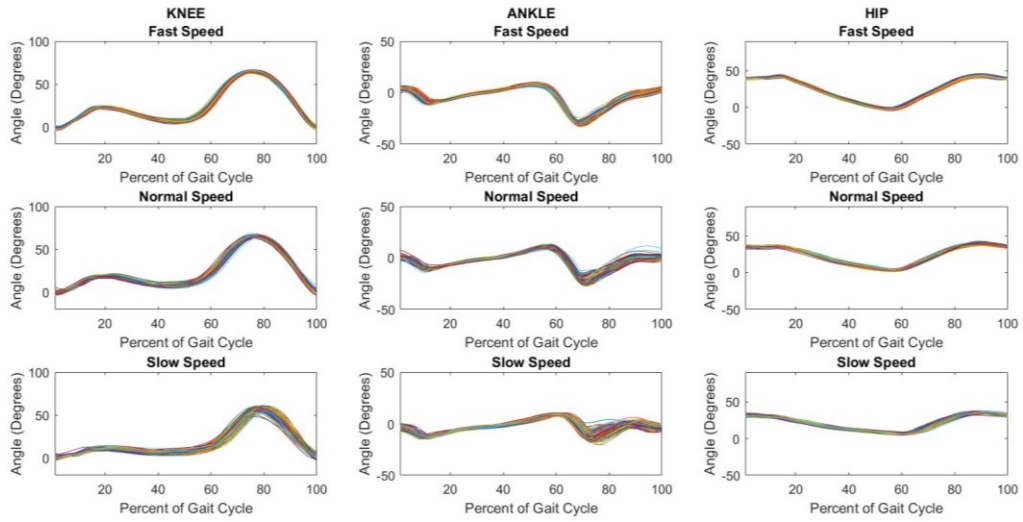


Figure 5.13 - Vicon angles of the lower limb (Subject 2).

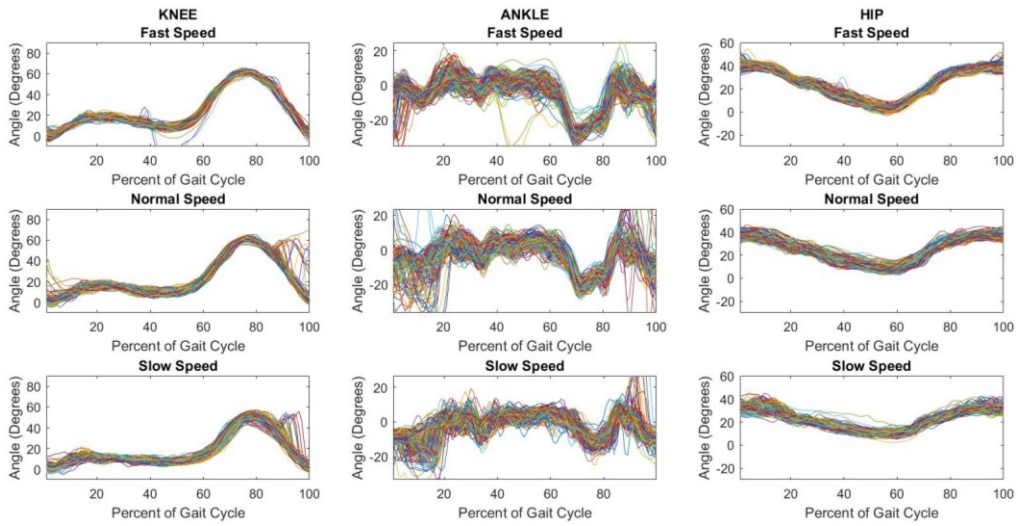


Figure 5.14 - OpenPose angles of the lower limb (Subject 2).

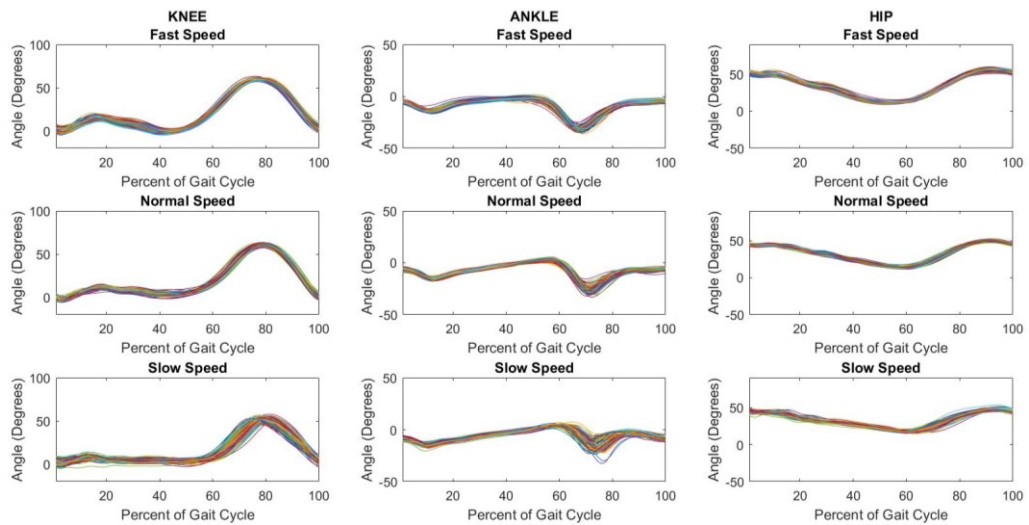


Figure 5.15 - Vicon angles of the lower limb (Subject 3).

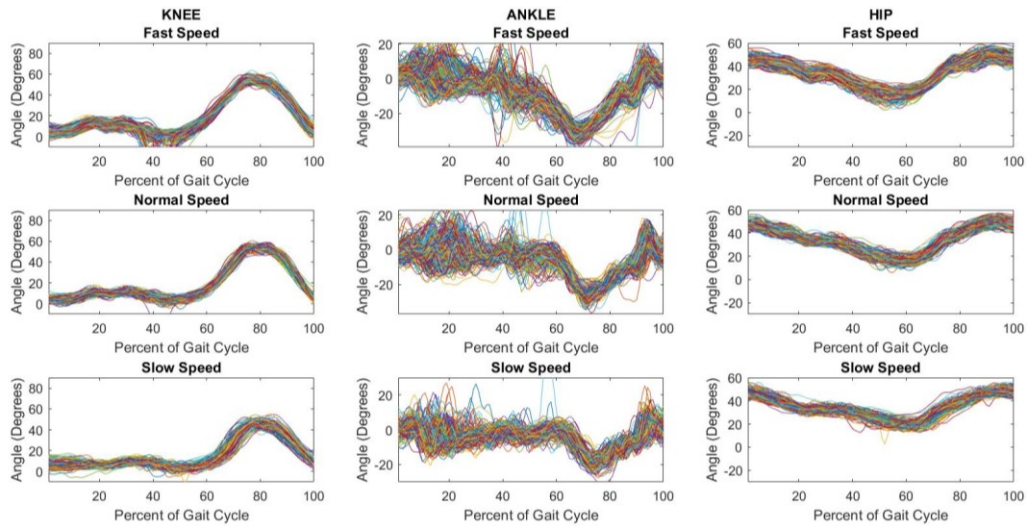


Figure 5.16 - OpenPose angles of the lower limb (Subject 3).

Through the data obtained by the OpenPose tool, the angles for each subject analyzed were calculated using the model defined in Paragraph 4.3.3.2. The latter are compared with the angles obtained directly from the Vicon instrument, in Figure 5.17 and Figure 5.19 the median, and the standard deviation of the trend of the angles in the two systems are shown using the different steps available for each subject. Instead, Figure 5.18 and Figure 5.20 show the median distance and the corresponding standard deviation obtained by comparing the angles extracted for both systems.

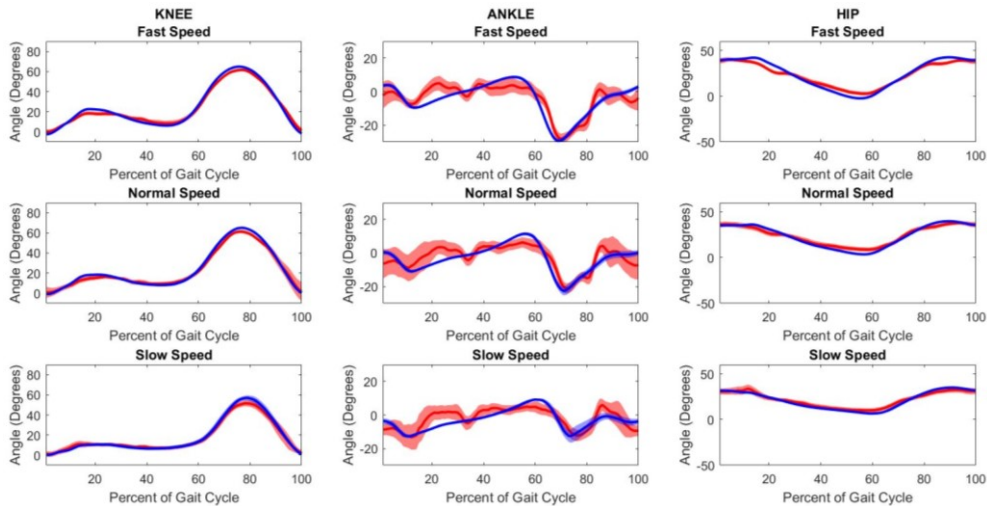


Figure 5.17 - Hip, Knee and Ankle angles obtained by Vicon system, in blue, and OpenPose angles, in red (Subject 2).

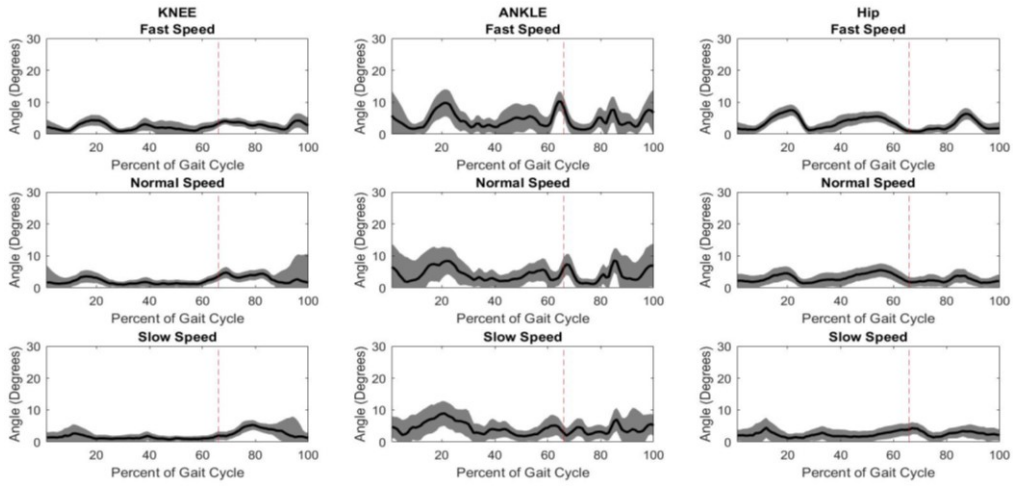


Figure 5.18 - Median distance, in black, and standard deviation, in grey, between the angles provided by the two systems (Subject 2).

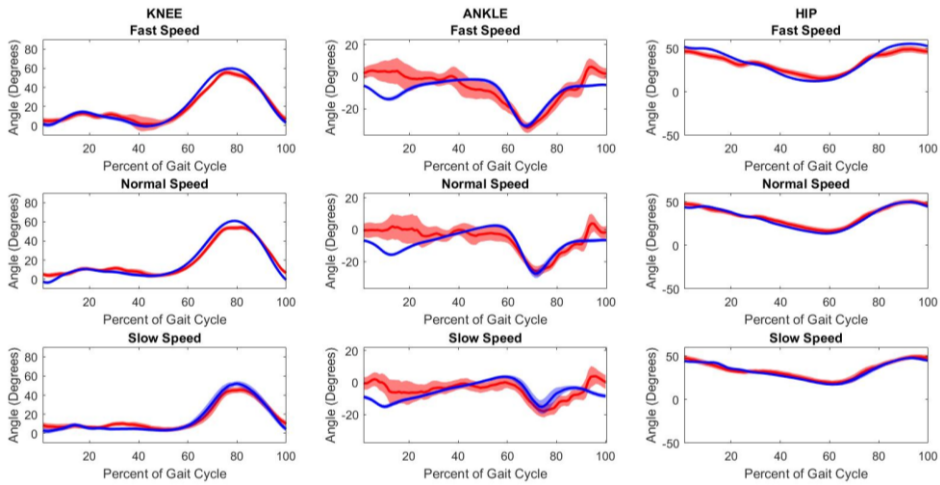


Figure 5.19 – Lower limb angles obtained by Vicon system, in blue, and OpenPose angles, in red (Subject 3).

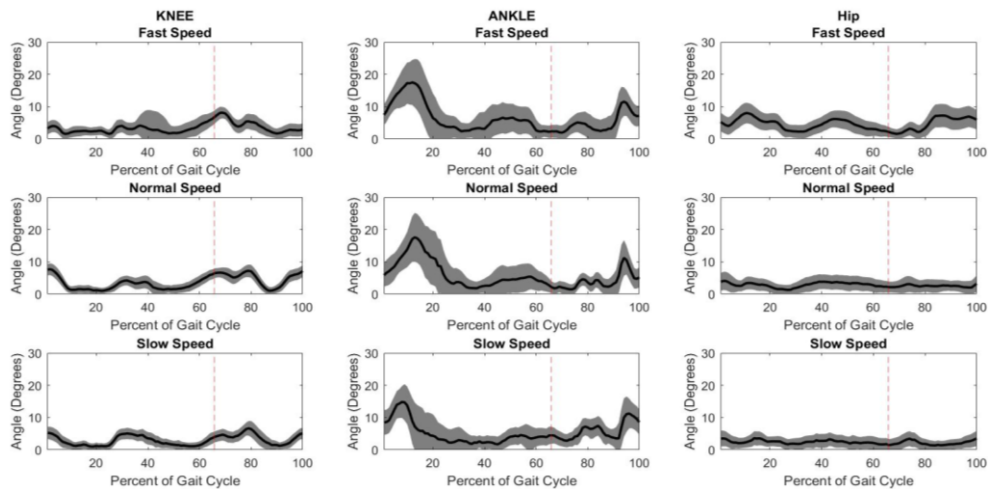


Figure 5.20 - Median distance, in black, and standard deviation, in grey, between the angles provided by the two systems (Subject 3).

In the same way, as in the evaluation made in Paragraph 5.1, the Mean Absolute Errors and the Root Mean Square Errors are calculated, for each step, between the angles of the gait cycle provided by the Vicon system and the angles obtained from the OpenPose coordinates.

Figure 5.21, Figure 5.22 and Figure 5.23 show the MAE values and the standard deviation calculated for the angles, respectively, of the hip, knee, and ankle in the three different speeds of the trials and for each subject.

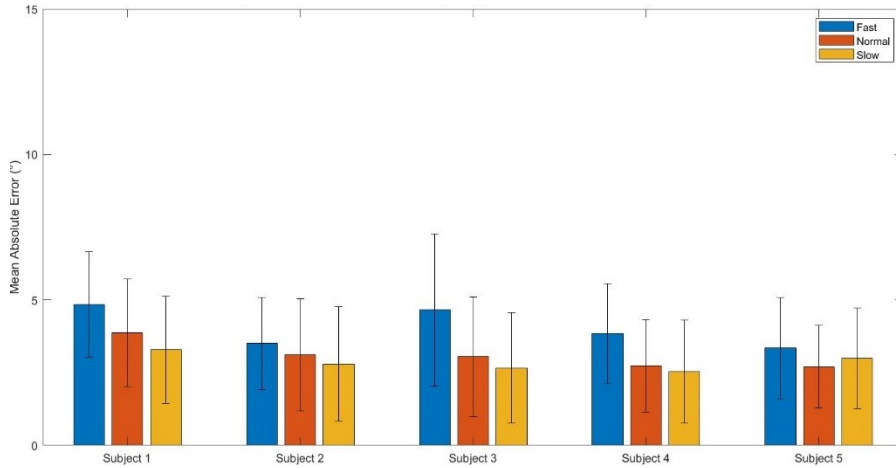


Figure 5.21 – MAE of the Hip angles of all subject in the different speed level of walking trial.

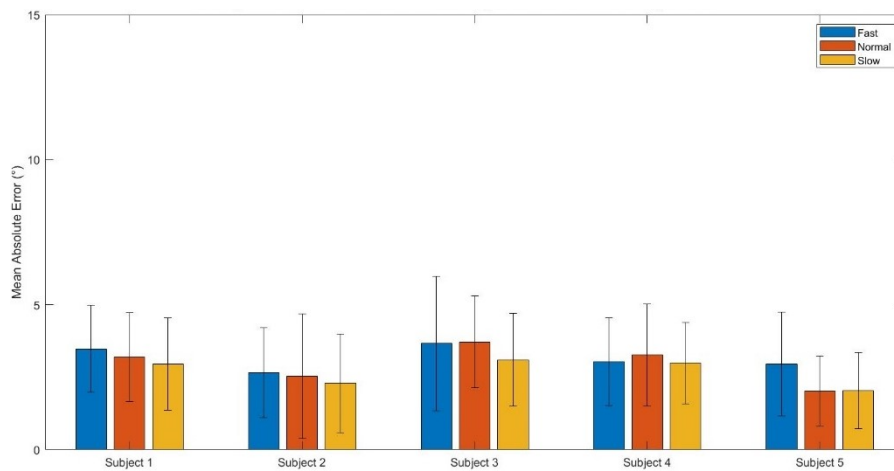


Figure 5.22 – MAE of the Knee angles of all subject in the different speed level of walking trial.

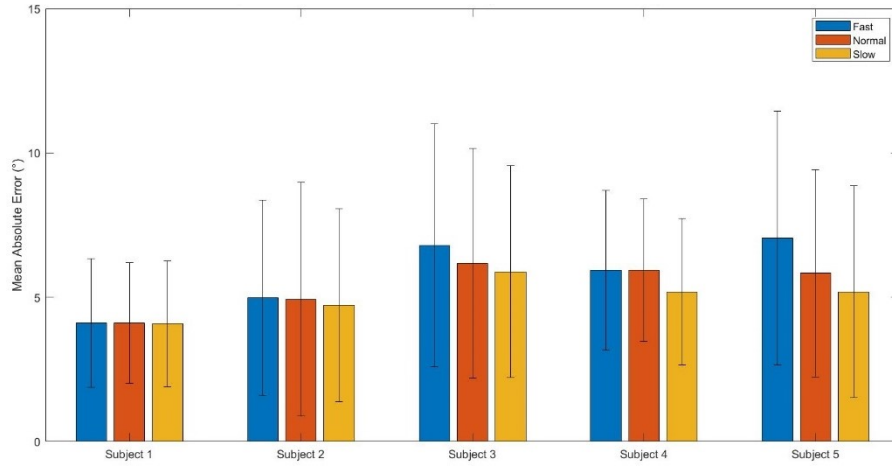


Figure 5.23 - MAE of the Ankle angles of all subject in the different speed level of walking trial.

Table 5.8 and Table 5.9 show the results obtained for the five subjects; in particular, the first table shows the average values of the distances obtained in the gait cycle between the hip, knee, and ankle angles provided by the Vicon system and the same angles obtained from the reference points provided by OpenPose, and the second table instead shows the mean value of the Root Mean Square Error calculated considering the two methods.

Table 5.8 – Average values of MAE between Vicon and OpenPose angles.

		Subject				
		1	2	3	4	5
Mean	Hip angle	4.00	3.14	3.46	3.04	3.02
MAE	Knee angle	3.21	2.50	3.49	3.10	2.34
(°)	Ankle angle	4.10	4.88	6.29	5.69	6.02

Table 5.9 – Average RMSE values obtained from Vicon and OpenPose angles.

		Subject				
		1	2	3	4	5
Mean	Hip angle	4.75	3.85	4.31	3.69	3.71
RMSE	Knee angle	4.00	3.21	4.32	3.68	3.11
(°)	Ankle angle	4.81	6.27	8.42	7.18	7.92

The correlation between the joint angle curves of the two systems was studied through the Pearson correlation coefficient. In this case, it is calculated using the formula:

$$P_{coeff} = \frac{\sigma_{\gamma_V \gamma_{OP}}}{\sigma_{\gamma_V} \sigma_{\gamma_{OP}}} \quad (5.6)$$

Where γ_V and γ_{OP} correspond respectively to the mean time series of the hip, knee, and ankle angles extracted with the two systems. The coefficients were calculated for each subject and for each session performed by it. Table 5.10 shows the final values of the index

correlation, for each subject the final value of the coefficient of each angle was obtained by taking the averaging the coefficients of the different sessions.

Table 5.10 - Average Pearson Coefficient values obtained from Vicon and OpenPose angles.

		Subjects				
		1	2	3	4	5
Pearson coefficient	Hip angle	0.963	0.960	0.959	0.982	0.966
	Knee angle	0.988	0.984	0.979	0.993	0.991
	Ankle angle	0.877	0.683	0.513	0.752	0.740

To evaluate the quality of the correlation indices, Figure 5.24 shows the linear fitting graphs obtained by placing in the abscissa the trajectories of the angles obtained by the Vicon system in the different sessions and not subdivided into steps and ordinates the corresponding trajectories of the angles calculated with the method proposed through the coordinates of OpenPose. In fact, in this case, the amount of data considered for the fitting is greater but despite this, the values obtained, for the subject in question, of R-square are always close to 1 and the RMSE values are less than 2 degrees for all the three angles.

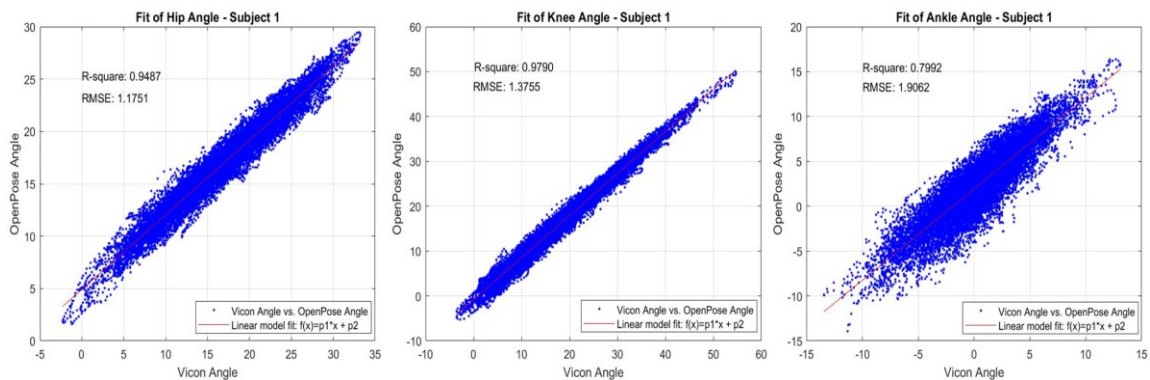


Figure 5.24 - Fit curves and goodness-of-fit info for the angles of hip, knee, and ankle of the two systems for subject 1.

The four initial figures (Figure 5.13, Figure 5.14, Figure 5.15 and Figure 5.16) are very important as they show the trend of the angles obtained with the two different systems. In fact, it is immediately evident that the angles of the hip, knee, and ankle obtained with the coordinates of the OpenPose system are noisier, especially as regards the angle of the ankle. The trend of this angle is not only noisier than that obtained by the Vicon system but also has a different trend for each step of the subject. This can be attributed to a high noise present in the coordinates of the ankle and medial foot, which are the markers used to calculate this angle, extracted with the OpenPose system but also to an imprecise prediction of these by the instrument.

As can be seen from Figure 5.21, Figure 5.22 and Figure 5.23, in general, despite the different speeds, there is always an error of fewer than 8 degrees in the angles of the hip, knee, and ankle for all subjects. Furthermore, it is evident that in all three angles of the lower limb the greatest errors are in the Fast speed of the walking trials, this is not surprising as it is expected that the OpenPose tool is not able to correctly identify the key-points when the subjects move faster. As for the hip angles, the maximum error that is committed is equal to 4.85 degrees in the Fast session of the third subject. Also, the maximum knee error value occurs in the same session of the same subject and is equal to 3.71 degrees. In general, the highest values of errors are obtained for the ankle angles up to a maximum of about 7 degrees.

Table 5.8 shows the average values of the errors relative to each angle of each subject. It is immediately noted that as regards the hip angle this always has an average error value of fewer than 4 degrees. It can be said that it is a quite satisfactory result for this angle because, in general, the hip joint is the most difficult to identify by the OpenPose system, especially during the walk in the lateral view where it can sometimes be obscured by the upper limbs of the subject. Furthermore, it is also noted from Figure 5.17 and Figure 5.19 that the trend of this angle is similar to that extracted from the Vicon system, this is also confirmed by the values very close to the unit of the Pearson coefficients calculated for this angle. In fact, it can be said that between the hip angles of the two systems there is a strong correlation.

Even more evident is the goodness of the results obtained for the knee angles. Indeed, Table 5.8 shows an MAE of less than 3.5 degrees for all subjects. Also, in this case, as can be seen in Table 5.10, the Pearson correlation indices denote a strong correlation between the knee angles obtained in the two systems.

It is manifest from Figure 5.17 and Figure 5.19 that the ankle angle extracted with the simplified biomechanical model through the joint data predicted by the OpenPose system is the one that has a trend that differs most from the trend obtained with the gold standard. In fact, the average MAE has a higher value than the other two angles, always remaining below 7 degrees. Also in regard to the evaluation from the statistical point of view, there is a strong correlation only in three subjects, in the first, in the fourth, and in the fifth, with values at the lower limit of the interval, as shown in Table 5.10. However, the remaining subjects have a moderate correlation.

Table 5.9 shows the average RMSE values obtained from the Vicon angles and the OpenPose angles and also in this case the same considerations made for the MAE average can be made. Both for the hip and knee angles the RMSE value is always below 5 degrees, however, for the ankle angle, it reaches a maximum of about 8.5 degrees.

It is important to remark that a portion of the estimation errors discussed above is due to the different biomechanical models used to compute the angles, as shown in the validation analysis described in Paragraph 5.1. The error due to the model used to derive the angles contributes up to 3 degrees for certain angles.

5.4 Kinematics Parameters

In addition to the assessments regarding the angles and centers of rotation of the right lower limb, the kinematic parameters of the joint movements in the sagittal plane were evaluated. From the point of view of clinical gait analysis, it is important to evaluate the reliability of specific kinematic parameters extracted from the curves of the lower limb angles as well as verifying their trends in the two systems. The parameters were extracted by selecting the crucial points of the corner curves, such as maxima or minima in the main steps of the step or values in particular points of the step cycle, and their occurrence expressed as a percentage of the gait cycle [21].

In particular, ten kinematic parameters relating to certain events of the Gait Cycle were compared. For the hip angle, the following were evaluated:

- Flexion at heel Contact (H1),
- Minimum flexion in stance phase (H2),
- Maximum flexion in swing phase (H3).

For the knee angle:

- Flexion at heel Contact (K1),
- Maximum flexion at loading response (K2),
- Maximum extension in stance phase (K3),
- Maximum absolute flexion of the swing phase (K5).

Finally, for the ankle angle:

- Flexion at heel Contact (A1),
- Maximum plantar flexion (A2),
- Maximum dorsiflexion in stance phase (A3).

For each step of the angles, both Vicon and OpenPose, the kinematic parameters have been extracted so that they can be compared both in terms of their value and their position within the gait cycle. The kinematic parameters of the angles that highlighted the Heel Contact event were excluded from the comparison between the positions, as the same RHS and RTO events were used to divide the angles of the two systems into steps.

Figure 5.25 shows the curves concerning the angles of the hip, knee, and ankle at different speeds, and the respective kinematic parameters are highlighted with dots.

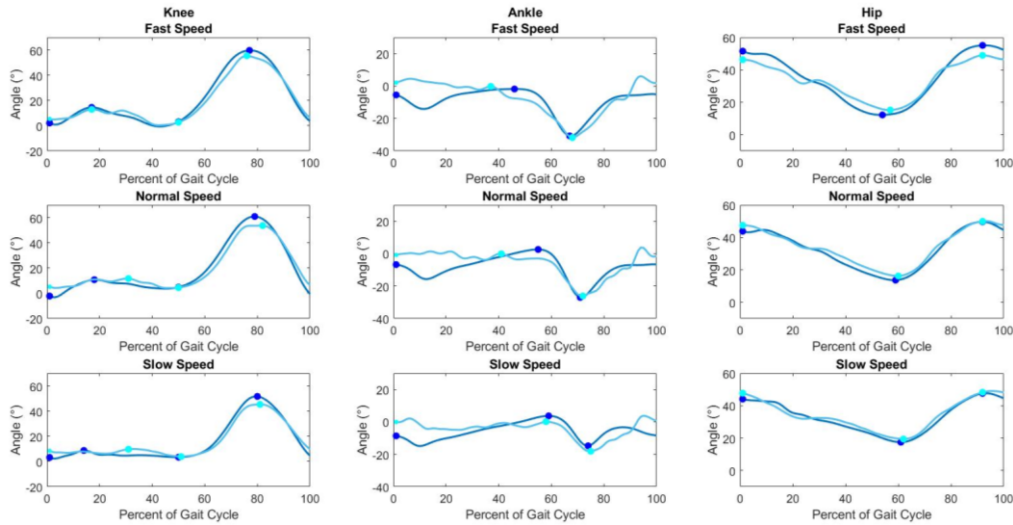


Figure 5.25 - Comparison of the Kinematic Parameters for the subject 3. In blue the curves of the angles extracted with the Vicon system and in dark blue dots the parameters are highlighted, in light blue the curves and parameters obtained with the data extracted from the OpenPose system.

Subsequently, the Mean Absolute Errors are calculated both between the values assumed by the parameters in the angles of the two systems and from the position of the kinematic parameters identified, both using equation 5.2.

Figure 5.26 shows for each speed of the subject the MAE between the parameters' values of the angles obtained with the Vicon system and the angles calculated with the proposed method using the OpenPose data.

Table 5.11 shows the average values of the MAE, for each subject, of the angular values assumed by the kinematic parameters obtained from the angles of the two systems.

Table 5.12 shows the absolute errors between the positions in the Gait Cycle of the kinematic parameters identified in the corners of the two systems.

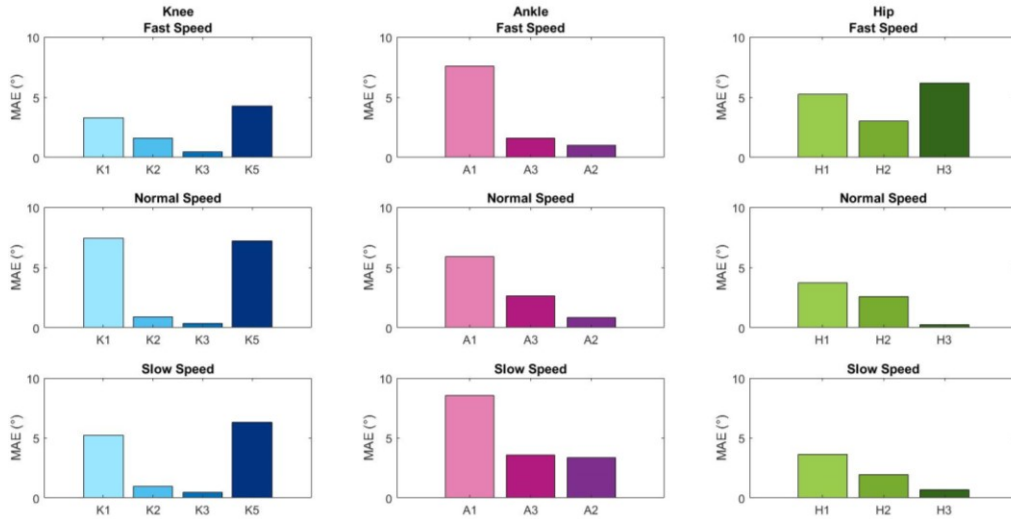


Figure 5.26 - MAE values obtained by comparing the extracted parameters values for the angles of the two systems for the subject 3.

Table 5.11 - MAE of the values of the kinematic parameters obtained from the corners of the lower limb extracted with the two systems of motion tracking.

		Subjects				
		1	2	3	4	5
MAE (°)	H1	2.17	0.64	4.20	1.07	1.73
	H2	4.73	4.57	2.51	4.61	3.91
	H3	4.58	2.70	2.37	3.53	4.42
	K1	0.85	2.11	5.31	4.71	5.06
	K2	3.06	2.33	1.15	1.71	1.67
	K3	0.66	0.95	0.42	2.75	0.97
	K5	5.86	4.14	5.93	5.26	2.58
	A1	0.48	6.91	7.35	4.10	4.27
	A2	3.07	0.95	1.75	4.13	4.17

Table 5.12 - MAE of the position in the GC of the kinematic parameters of the angles of the two system.

		Subjects				
		1	2	3	4	5
MAE (%)	H2	3	2	2	0	2
	H3	1	2	0	1	0
	K2	9	3	10	3	5
	K3	0	0	0	0	0
	K5	1	1	2	1	1
	A3	2	6	8	5	8
	A2	5	1	1	2	2

As represented in Table 5.11, an error was obtained from the comparison of the kinematic parameters of the angles extracted from the two systems which in general is always less than 5 degrees except for parameters K1, K5, and A1. Therefore, the parameters concerning the hip angles are particularly acceptable and this is also confirmed in Table 5.12 where it is evident that the error made in identifying these parameters is negligible. In the same table, on the other hand, there is an error in the position of the parameters with a maximum of 10 for the parameter concerning the maximum flexion of the knee in the stance phase (K2). This is even more evident in Figure 5.25 where substantially in the angle extracted from the OpenPose system the maximum flexion is found in a position at the limit of the stance phase, this is because the knee angle curve obtained with the OpenPose data is a little noisier and has artifacts than the Vicon system.

As for the kinematic parameters of the ankle angle, the error obtained was expected because the curves in the two systems are the ones that differ most, moreover, that of the OpenPose system is the noisiest as can be seen in Figure 5.25. In fact, even as regards the position of parameters A2 and A3, a high error is obtained up to a maximum of 8.

Chapter 6

6 Conclusion and Future Goals

The goal of this thesis markerless project was precisely to understand if it is possible to carry out gait analysis through a pose estimation algorithm based on deep-learning. In fact, if on one hand there is the analysis based on optoelectronic stereophotogrammetry, which is the most accurate available today and is considered the gold standard in gait analysis laboratories, on the other hand, there is the growing need to use new technologies to cut the analysis time and the costs but also to meet the needs of subjects with motor disabilities, making the assessment as comfortable as possible without impacting the accuracy of the results.

In order to reach this goal, a comparison was made between the gait analysis carried out through one of the systems considered gold standard (Vicon), and a novel markerless 2D estimation tool of the human body key-points (OpenPose). As already shown in chapter 4, a pre-processing of the data obtained by OpenPose was carried out together with the creation of ad-hoc model to calculate the angles of the lower limb.

In particular, data collected by 5 healthy subject walking at different speeds on a treadmill were analyzed. The comparison was based on three main fronts: the position of the articular centers of rotation in the two systems; the angles of the hip, knee, and ankle obtained directly from the Vicon system and the corresponding calculated with the data extracted from the OpenPose tool; and, finally, the kinematic parameters of the gait cycle of each subject.

The analysis carried out on the position of the joint centers did not show a consistent error in the OpenPose's estimate. The greatest differences, in terms of distance, appeared exclusively on the key-points of the neck, ankle and feet. This is not to be considered as an estimation error of the OpenPose framework but more like a discrepancy of reference points at an anatomical level. The only exception is for the hip marker, where there is a greater distance in its trajectory along the x-axis. This can be considered as an error that arises from the lack of information by OpenPose in this anatomical area since is not very visible and identifiable from the lateral and it suffers from occlusions derived from the subject's arm swing. Despite these differences, the statistical analysis however confirmed a high correlation, and therefore similarity, between the trajectories along the two axes of the markers that were considered in this work.

As for the angles of the lower limb, the method used to extract them was validated and was considered quite robust because it showed a Root Mean Square Error of less than 3.5 degrees for all three angles (hip, knee, and ankle).

As for the comparison between the hip, knee, and ankle angles of the two systems, the error obtained is always less than 8.5 degrees. Precisely, for the knee angle, an RMSE of less than 4.5 degrees is obtained for all subjects and for all the speeds of the walking trials performed. For the hip angle, there is an RMSE of less than 5 degrees, this is a remarkable result if we consider that, in general, this angle is very difficult to estimate given its position which is not always perfectly evident. And the goodness of these two angles is always confirmed, for all the subjects analyzed, by the Pearson correlation index which indicates a strong correlation.

For the ankle angle, the error is greater in fact it reaches 8.5 degrees in the worst case. Although it is always below 10 degrees, the result is not very satisfactory as this angle, together with that of the knee, is the easiest to evaluate. The origin of this error was therefore investigated, which can substantially refer to a high oscillation of the foot and ankle markers used for calculating the angle and therefore to an imperfect estimate by the OpenPose tool. In fact, with the exception of the first subject for which an RMSE of less than 5 degrees is obtained, in the other cases, the error is greater but also the trend of the angle along the gait cycle is different from that obtained by the Vicon system. The reason for the high oscillation especially of the foot markers that caused an error in the calculation of the ankle angle is essentially due to the color of the shoes of the other four subjects. In fact, these latter subjects have a very dark shoe color and very similar to that of the treadmill and this does not allow OpenPose, which is an optical system, to properly identify the foot and therefore also to adequately estimate positions of the key points of the foot in each frame (specifically the Medial Toe, which is the marker that was used for the calculation of the ankle angle). In fact, the good quality of the angle obtained in the first subject is due to the use of light-colored shoes.

Therefore, the use of OpenPose should not be underestimated but it must be taken into account that perhaps the protocol needs to be improved (such as the use of shoes of a different color from that of the treadmill) to allow a more precise and accurate analysis.

Additionally, the estimation errors observed in this comparison include the error resulting for the use of a simplified biomechanical model for the OpenPose data, which the validation analysis quantified in the extent of approximately 3 degrees. This highlights the need to further improve the markerless system on multiple fronts. On one hand, it is necessary to increase the accuracy of the key-point estimation, reduce the artifacts from motions and occlusions and define better acquisition protocols; on the other hand, a more sophisticated biomechanical model for the angle estimation is needed to reduce the impact on the error derived by the adoption of a simple method for computing the angles in the OpenPose case.

Finally, the comparison of the kinematic parameters of the angles of the lower limbs obtained with the two systems was carried out both on their value and on their position within the GC. A Mean Absolute Error was obtained for the value of the parameters which is always less than 6 degrees for those relating to the hip and knee angles and less than 7.5

degrees for those of the ankle angle. As far as their position is concerned, the difference is mainly due to the artifacts present in the angles calculated with the OpenPose data.

In conclusion, it can be stated that the use of OpenPose for rehabilitation medicine is not yet possible as it is not extremely accurate but also because, in this work, it was used exclusively on subjects who did not have any type of motor disability and anomaly in the gait. Therefore, a more in-depth research is needed that aims at addressing the problems that emerged in this work. Despite the limitations, the obtained results are promising and are a solid basis for future studies.

Furthermore, during this work, different methodologies were used to fulfill the purpose of the thesis and which could be interesting if further investigated for a subsequent study. The first method we tried to use is based on inverse kinematics as this is a method for calculating posture by estimating every single degree of freedom. But precisely because the methods generally used suffer from high computational costs and can produce unrealistic poses, we have chosen to use a heuristic method, Forward And Backward Reaching Inverse Kinematics (FABRIK), that does not use angles of rotation or matrices but finds the position of each joint by identifying a point on a line, managing to converge in a few iterations [22]. Although promising, with this methodology we have not been able to obtain satisfactory results as the method does not consider the angular rotation constraints linked to each joint and in many cases, it was unable to reproduce real positions. Furthermore, although the reference document expressed the possibility of inserting constraints, its application in a real-case scenario resulted complex and time-consuming. Despite this, it is believed that the use of an inverse kinematics method, perhaps not simplified, could help to obtain better results.

Moreover, another technique that has been tried to reduce the oscillations of the articular centers is based on the use of the Kalman filter [23]. Specifically, an extended Kalman filter was used in a very simple version with a constant acceleration model with additive noise. The state vector had inside it the positions, velocities, and accelerations of the joint coordinates, the matrix generally used for a filter with the constant acceleration model was used as process noise [24], and as measurement noise, it was held account of the confidence value of each key-points obtained in output from the OpenPose system. However, the results obtained did not make a significant contribution precisely because the constant acceleration model was not effective because it was too simple and because it does not correspond to the kinematic model of the gait cycle. A model based on joint kinematics would be needed so that the filter can efficiently predict joint positions or even calculate angles directly from joint coordinates. In addition, a model that integrates constraints for greater efficiency, as well as better modeling of both measurement and process noise, would also be needed for better results. In general, the idea has the potential to improve system performance, but it needs to be explored further.

Bibliography

- [1] Z. Abu-Faraj, G. Harris, P. A. Smith e S. Hassani, «Human Gait and Clinical Movement Analysis,» *Wiley Encyclopedia of Electrical and Electronics Engineering*, vol. Second Edition, pp. 1-34, 2015.
- [2] A. Kharb, V. Saini, Y. Jain e S. Dhiman, «A review of gait cycle and its parameters,» *IJCEM International Journal of Computational Engineering & Management*, n. 13, p. 78–83, 2011.
- [3] P. Calderale e C. Bignardi, «Biomeccanica dell'articolazione dell'anca,» *Biomeccanica Ortopedica e Traumatologica*, p. 193–207, 1995.
- [4] M. Nordin e V. H. Frankel, *Basic Biomechanics of the Musculoskeletal System*, Chapter 7: Biomechanics of the knee, IV a cura di, Philadelphia: Lippincott Williams & Wilkins, 2012.
- [5] H. G. Chambers e D. H. Sutherland, «A Practical Guide to Gait Analysis,» *The Journal of the American Academy of Orthopaedic Surgeons*, vol. 10, n. 3, 2002.
- [6] G. Severini, M. Manca, G. Ferraresi, L. M. Caniatti, M. Cosma, F. Baldasso, S. Straudi, M. Morelli e N. Basaglia, «Evaluation of Clinical Gait Analysis parameters in patients affected by Multiple Sclerosis: Analysis of kinematics,» *Clinical Biomechanics*, vol. 45, pp. 1-8, 2017.
- [7] R. Caldas, M. Mundt, W. Potthast, F. B. d. L. Neto e B. Markert, «A systematic review of gait analysis methods based on inertial sensors and adaptive algorithms,» *Gait & Posture*, vol. 57, pp. 204-210, 2017.
- [8] C.-Y. Hsu, Y.-S. Tsai, C.-S. Yau, H.-H. Shie e C.-M. Wu, «Test-Retest Reliability of an Automated Infrared-Assisted Trunk Accelerometer-Based Gait Analysis System,» *Sensors*, vol. 16, 2016.
- [9] A. Muro-de-la-Herran, B. Garcia-Zapirain e A. Mendez-Zorrilla, «Gait Analysis Methods: An Overview of Wearable and Non-Wearable Systems, Highlighting Clinical Applications,» *Sensors*, vol. 14, pp. 3362-3394, 2014.
- [10] M. Galli, V. Cimolin, V. Crugnola, L. Priano, F. Menegoni, C. Trotti, E. Milano e A. Mauro, «Gait pattern in myotonic dystrophy (Steinert disease): A kinematic,

- kinetic and EMG evaluation using 3D gait analysis,» *Journal of the Neurological Sciences*, vol. 314, p. 83–87, 2012.
- [11] R. Baker, «Gait analysis methods in rehabilitation,» *Journal of NeuroEngineering and Rehabilitation*, 2006.
- [12] R. A. Guler, N. Neverova e I. Kokkinos, «DensePose: Dense Human Pose Estimation In TheWild,» *Proceedings of the IEEE Conference on Computer Vision and Pattern Recognition*, pp. 7297-7306, 2018.
- [13] Z. Cao, G. Hidalgo, T. Simon, S.-E. Wei e Y. Sheikh, «OpenPose: Realtime Multi-Person 2D Pose Estimation Using Part Affinity Fields,» *IEEE Transactions on Pattern Analysis and Machine Intelligence*, vol. 43, 2021.
- [14] «3D Body (Skeletal) Tracking Middleware: NuiTrack SDK,» [Online]. Available: <https://nuitrack.com/>.
- [15] *MATLAB, version R2020a*, Natick, Massachusetts: The Math Works Inc, 2010.
- [16] «Calibration Motion Capture Accessories,» [Online]. Available: <https://www.vicon.com/products/vicon-devices/calibration>.
- [17] «Vicon Nexus User Guide,» [Online]. Available: [https://docs.vicon.com/..](https://docs.vicon.com/)
- [18] «Plug-in Gait Reference Guide,» [Online]. Available: [https://docs.vicon.com/..](https://docs.vicon.com/)
- [19] «Visual 3D Professional - Biomechanics Research Tools,» [Online]. Available: <https://www.visual-3d.com/>.
- [20] «What Is Camera Calibration?,» [Online]. Available: <https://www.mathworks.com/help/vision/ug/camera-calibration.html>.
- [21] M. G. Benedetti, F. Catani, A. Leardini, E. Pignotti e S. Giannini, «Data management in gait analysis for clinical applications,» *Clinical Biomechanics*, vol. 13, pp. 204-215, 1998.
- [22] A. Aristidou e J. Lasenby, «FABRIK: A fast, iterative solver for the Inverse Kinematics problem,» *Graphical Models*, p. 243–260, 2011.
- [23] R. E. Kalman, «A New Approach to Linear Filtering,» *Journal of Basic Engineering*, pp. 36-45, 1960.
- [24] P. Das, K. Chakravarty, A. Chowdhury, D. Chatterjee, A. Sinha e A. Pal, «Improving joint position estimation of Kinect using anthropometric constraint

based adaptive Kalman filter for rehabilitation,» *Biomedical Physics & Engineering Express*, 2018.

- [25] W. Pirker e R. Katzenschlager, «Gait disorders in adults and the elderly,» *Wien Klin Wochenschr*, n. 129, p. 81–95, 2017.